Simulated Rotor Wake Interactions Resulting from Civil Tiltrotor Aircraft Operations Near Vertiport Terminals

Larry A. Young[1]
Gloria K. Yamauchi[2]
NASA Ames Research Center, Moffett Field, CA, 94035

Ganesh Rajagopalan[3]
Sukra-Helitek, Inc. and Iowa State University, Ames, IA 50011

A mid-fidelity computational fluid dynamics tool called RotCFD – specifically developed to aid in rotorcraft conceptual design efforts – has been applied to the study of rotor wake interactions of civil tiltrotor aircraft in the immediate vicinity of vertiport/airport ground infrastructure. This issue has grown in importance as previous NASA studies have suggested that civil tiltrotor aircraft can potentially have a significant impact on commercial transport aviation. Current NASA reference designs for such civil tiltrotor aircraft are focused on a size category of 90-120 passengers. Notional concepts of operations include simultaneous non-interfering flight into and out of congested airports having vertiports, that is, prepared VTOL takeoff and landing zones, or underutilized short runways for STOL operation. Such large gross-weight vehicles will be generating very high induced velocities. Inevitably, the interaction of the rotor wake with ground infrastructure such as terminal buildings and jetways must be considered both from an operational as well as design perspective.

Nomenclature

C_p	=	pressure coefficient
C_T	=	rotor power coefficient
C_T	=	rotor thrust coefficient
FM	=	rotor hover figure-of-merit
FM_∞	=	rotor hover figure-of-merit out-of-ground-effect
h/R	=	ratio of rotor height-above-ground with respect to rotor radius
v_w	=	wind speed
x/R	=	ratio of rotor horizontal-distance from vertical wall/plane, or correspondingly building, to rotor radius
$\Delta\varphi$	=	relative angular orientation of rotors to vertical wall/plane, or correspondingly building; with zero deg. orientation, the rotors are parallel to the wall/building.
$\Delta\psi$	=	relative direction of wind with respect to aircraft; zero deg. is towards the aircraft nose.

I. Introduction

IT has long been envisioned that rotorcraft in general, and tiltrotor aircraft in particular, might one day provide a significant role in commercial transport aviation. Several NASA-sponsored studies over the past two decades have reinforced this vision of commercial transport rotorcraft. Recent studies, Refs. 1-3, have focused on tiltrotor aircraft in the size category of 90-120 passengers. Such studies have shown that large civil tiltrotors can have a

---

[1] Aerospace Engineer, Aeromechanics Branch, Flight Vehicle Research and Technology Division, Mail Stop 243-12, AIAA Associate Fellow.

[2] Aerospace Engineer, Aeromechanics Branch, Flight Vehicle Research and Technology Division, Mail Stop 243-12.

[3] Professor, Department of Aerospace Engineering.

significant influence on reducing National Airspace System (NAS) delays and increasing throughput. To accomplish such gains it will be necessary to either develop and make use of vertiports (prepared VTOL takeoff and landing zones) and short underutilized runways at congested airports. Figure 1 is a simple illustration of a notional airport layout in which there is both a vertiport terminal and short runway for tiltrotor operations. A major consideration in the development of vertiports co-located at airports is the magnitude of rotor/wake interactions (i.e. in-ground-effect groundwash) from such large vehicles in close proximity to ground infrastructure.
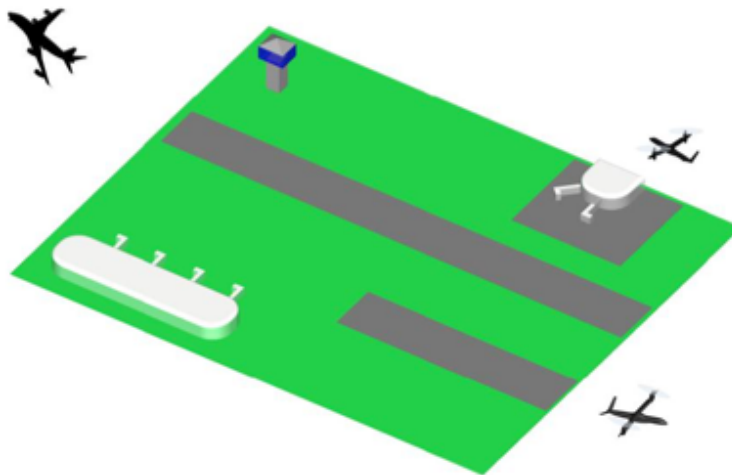
Figure 1. On-Airport-Property Vertiport Tiltrotor Operations (VTOL and STOL).

II. Scope of the Problem

In order to assess the compatibility of the NASA civil tiltrotor (CTR) reference designs with the anticipated Concept of Operations (CONOPS) of such aircraft operating into and out of major congested airports (circa ~2025) it is necessary to use computational fluid dynamics (CFD) tools to predict rotor/wake interactions, particularly rotor groundwash, in the immediate vertiport/terminal area. The CFD tool of choice for this study is RotCFD. RotCFD is a mid-fidelity CFD tool aimed at conceptual design. The technical approach for this study is to begin with simple rotor in-ground-effect (IGE) predictions, then proceed to dual side-by-side rotor IGE predictions, followed by a complete LCTR2 aircraft (Ref. 6) IGE predictions, followed by introducing walls, planes and simple geometric shapes representing buildings, and then concluding with a LCTR2 aircraft operating near a more realistic modeling of a vertiport terminal facility. Figure 2 and 3 are representative RotCFD results for the LCTR2 reference design operating near a vertiport terminal building.

In parallel with the above set of predictions, RotCFD will be validated for this class of problem. The single- and dual-rotor IGE predictions can be compared to analytical results, e.g. Refs. 7, 9, 10, and to data from experimental studies similar to Ref. 8.
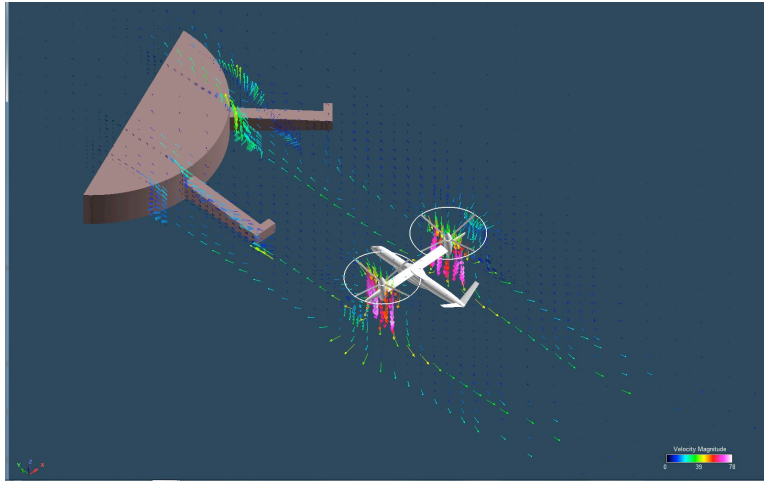
Figure 2. Representative Rotor/Wake Interaction for Civil Tiltrotor in vicinity of Vertiport (Velocity Vectors)
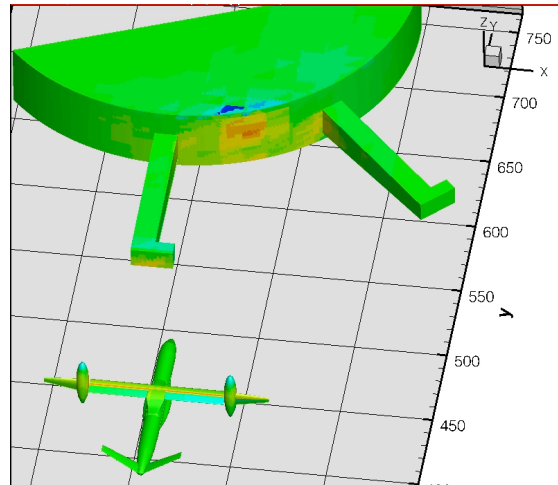

Figure 3. Representative Rotor/Wake Interaction for Civil Tiltrotor in vicinity of Vertiport (Surface Pressures on Aircraft and Building)

III.   Description of Analysis Approach

A. RotCFD Computational Fluid Dynamics Tool

RotCFD attempts to bridge the two worlds of design and Computational Fluid Dynamics (CFD) with the help of an Integrated Design Environment (IDE) specific to rotorcraft. RotCFD emphasizes user-friendliness and efficiency that streamline the design process from geometry to CFD solution. The key components of RotCFD are a geometry module, a semi-automated grid generation module, a flow-solver module, a rotor module, a flow visualization and analysis module, all integrated in one environment. The concept of rotor blades represented by momentum sources forms the basis of this aerodynamic simulation tool for rotorcraft. The rotor momentum sources are primarily a function of the local velocity of the flow and the two-dimensional airfoil characteristics of the rotor blades. The

American Institute of Aeronautics and Astronautics

Navier-Stokes equations and the blade element theory are coupled implicitly to yield a self-contained method for generating performance, as well as the near and far wake including all the aerodynamic interference inherent in a situation.

During initial design studies, parametric variation of vehicle geometry is routine. A simple geometry tool (modest CAD functionality) is offered to simplify geometry manipulation. The current version of RotCFD can read the body geometry in STL or Plot3D format. Also, some simple shapes (bodies of revolution) can be generated from within RotCFD. In addition to general transformations such as translation, rotation and scaling, parametric variation of the geometry is available to assist with the design. Graphical visualization is used to make the geometry manipulation user-friendly: the user is able to see a preview of the geometry change before committing the change.

The RotCFD Cartesian unstructured (hanging node) grid is economical to generate and can be completely automated. The cells that intersect the body, and all the cells that immediately surround the intersected cells are replaced by tetrahedra. The simple shape of the tetrahedron allows the grid to be morphed slightly in order to conform to the body. Thus the body conforming grid generator modifies a Cartesian octree grid (Cartesian here meaning all faces are aligned with the Cartesian planes) such that the grid will approximately conform to the surface of the body. The grid is approximate since the algorithm only considers the intersections between the surface geometry and the edges of the original grid. New surface faces are generated based on those edge-surface intersections instead of using the original polygons from the surface geometry. This approximate approach avoids the technical difficulties associated with maintaining the surface geometry exactly as it intersects the grid, and allows the development of a simpler and more robust algorithm with a much shorter development time. The approach also has the advantage that clean geometries are not required, only that they be closed surfaces.

The flow field of a rotor is complex; even an isolated rotor is dominated by the mutual, aerodynamic interference effects of the blades. Therefore, all simulation techniques, to be successful, must consider interference effects. Any numerical algorithm that solves the Navier-Stokes equations is adequate for obtaining the flow field. The SIMPLER/SIMPLE (Ref. 4) line of pressure-based algorithms is suitable for low speed flows and currently SIMPLE is used for solving the flow field in RotCFD. Additional details describing RotCFD are summarized in Ref. 5.

During the course of this work two different beta versions of RotCFD were employed: version 9.11 and 9.13. Version 9.11 provided only laminar flow only solutions and version 9.13 provided both laminar and turbulent solutions. The turbulence model in RotCFD 9.13 employed in this study was the "realizable k-e" model; for more details refer to Ref. 21. As appropriate, the particular RotCFD version number will be cited wherever results are presented.

B. The LCTR2 Reference Design Vehicle

The baseline vehicle design used in this study is a NASA reference design described in Ref. 6. The LCTR2 is a 90-passenger vehicle and has been used in many past studies. Alternate large civil tiltrotor vehicle conceptual designs are available, e.g. the vehicle designs detailed in Refs. 1-3, but the LCTR2 reference design is perhaps the most well known. The RotCFD models are based on LCTR2 CAD geometry files that have been recently used to fabricate small-scale wind tunnel models of the LCTR2 vehicle. The LCTR2 reference design is currently used within the NASA Rotary-Wing project to aid in guiding this project's technology portfolio. Accordingly, this paper also focuses on the LCTR2 model.

By way of an initial assessment of RotCFD's rotor performance predictive capability, Fig. 4 compares the RotCFD-predicted hover out-of-ground-effect (OGE) figure-of-merit curve against a figure-of-merit curve generated (and presented in Ref. 6) by the well-known CAMRAD II rotor comprehensive analysis code. CAMRAD II is a lifting-line/lifting-surface code using a free-wake model for the rotor wake. It, like RotCFD, uses C81 airfoil tables to calculate the sectional blade aerodynamic loads. As can be seen in Fig. 4, the RotCFD figure-of-merit results are generally comparable to the CAMRAD II results with the exception that the RotCFD results seem to predict rotor stall before CAMRAD II does. Extensive rotor/tiltrotor experimental data correlation (e.g. Ref. 20) with CAMRAD II predictions necessitated the incorporation of stall delay models in order to correctly predict the high-thrust rotor characteristics of tiltrotor proprotors. Figure 4 would suggest that future versions of RotCFD should also incorporate stall delay models in its rotor performance analysis to improve its overall predictive capability.
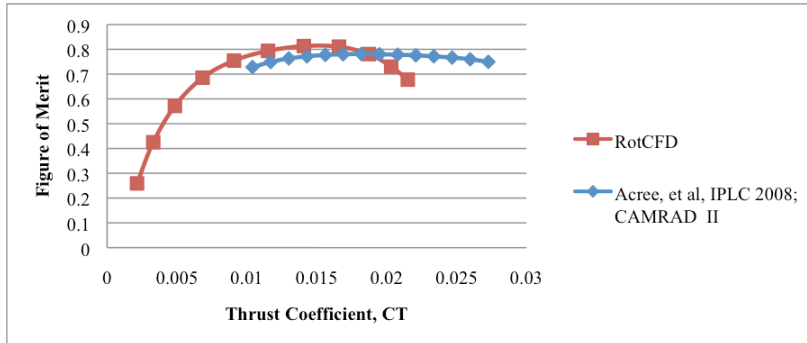
Figure 4. Comparison of LCTR2 Reference Design Isolated Rotor (Out-of-Ground Effect) Hover Performance Predictions

The Fig.4 RotCFD results should not be seen as significantly diminishing their utility for meeting the objectives of this study, which is that of studying rotor/wake interactions of tiltrotor aircraft with vertiport terminal buildings and airport surface infrastructure. Nevertheless, occasionally, some of the RotCFD results will be interpreted in the context of whether or not in-ground-effect performance has been influenced by predictions of premature rotor stall.

Throughout the main body of the paper, an attempt will be made periodically to show the RotCFD rotor/wake interaction results in the context of classic analytical results. These comparisons will hopefully help establish confidence in the general predictive capability of RotCFD for the rotor/wake interaction problem domain. Additionally, a concerted effort has been made to show in this paper's appendix experimental validation for RotCFD results against several pertinent rotor/wake interaction data sets from the literature.

C. Notional Terminal/Vertiport Layouts

The principal guide for vertiport design used in this study is Ref. 11. This FAA Advisory Circular, Ref. 11, has subsequently been canceled since its initial release in the mid-90's, but still represents the best source of vertiport design guidance available. The notional vertiport layout illustrated in Fig. 2-3 is somewhat inspired by certain terminals at Newark Liberty International airport. However, one of the key challenges of this study is to derive general results for rotor/wake interactions for CTR operating near vertiports and other airport ground infrastructure that are not unduly biased by the models used for such ground infrastructure. Therefore, in addition to, and before, presenting the vertiport modeling results a number of simpler modeling cases will be examined, including the influence of ground- and wall-planes on tiltrotor performance.

IV. Preliminary Results

The issue of rotor/wake interactions will be examined from the perspective of incrementally advancing from simple-to-complex modeling of the problem. In pursuing this methodical approach to increasing modeling complexity it is hoped that improved insights will be gained to the overall problem. Accordingly, RotCFD results will presented in the following incremental order: a single isolated (LCTR2) rotors in IGE and OGE hover; a single LCTR2 rotor in forward-flight IGE, third, dual LCTR2 rotors (with no wing or airframe) in hover IGE; a full

LCTR2 vehicle in hover IGE; a LCTR2 vehicle in hover in close proximity to both ground- and wall-planes; a LCTR2 vehicle yawed with respect to a wall-plane; a LCTR2 vehicle at several locations in close proximity to a vertiport, i.e. a simulated (Newark-like) terminal buildings; and, finally, a LCTR2 vehicle is close proximity to airport surface infrastructure and/or assets, specially a small general-aviation aircraft.

A. LCTR2 Rotor/Vehicle Configuration Build-Up and Parametric Sweeps

Figure __ presents a sequence of representative illustrations for the flow filed of a single rotor at several different heights above a ground-plane. The Fig. 5 results are for a LCTR2 rotor at a collective of twenty degrees. RotCFD is an unsteady Navier-Stokes analysis that is, in the case of hover OGE/IGE problems, being applied to flow problems that are intuitively seem steady in nature. Further, the RotCFD results presented in this paper are, for the most part, instantiations of the unsteady Navier-Stokes solution at the prescribed maximum time duration for the solution. This maximum time duration and the commensurate time steps specified were iterated upon during early test runs to insure that the rotor performance coefficients had asymptotically approached nominal value.

(a)

(b)
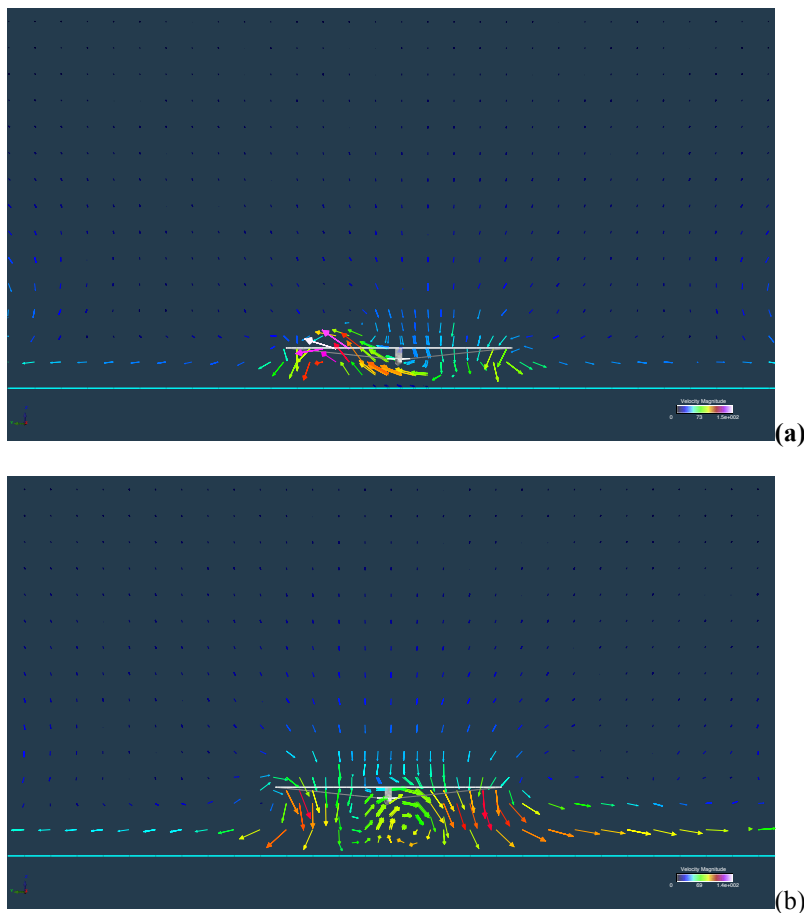
Figure 5. Single Rotor and Ground=Plane: (a) h/R = 0.25; (b) h/R=0.5.

American Institute of Aeronautics and Astronautics

Nonetheless, as can be seen in the Fig. 5 flow field images, there is considerable asymmetry (whereas intuitively symmetry is expected) observed in the hover IGE rotor flow, particularly at low values of h/R. At larger h/R values, the rotor wake does approach a symmetrical flow.

Figure 6 presents the accompanying rotor performance results in-ground-effect for the single LCTR2 rotor. RotCFD predictions were made for two different rotor collectives – ten and twenty degrees -- and thus rotor thrust levels. Also provided in Fig. 6 are two IGE performance trend curves for two classic rotor analyses, the work of Cheeseman and Bennett (Ref. 18) and the work of Hayden (Ref. 10).
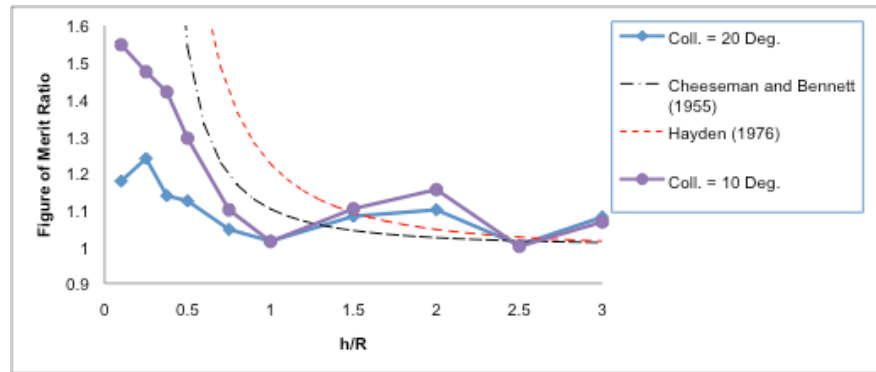
Figure 6. Single LCTR2 Rotor In-Ground-Effect at Two Different Collective Pitch Settings

Figure 7 illustrates the behavior of a single LCTR2 rotor IGE with freestream velocity of V=13 fps or 4 m/s, an effective advance ratio of μ=0.02. The "horseshoe" ground vortex at the forward edge of the rotor disk can be clearly seen in the velocity vectors mapping the rotor flow field and the velocity iso-surface in Fig.7a-b.

American Institute of Aeronautics and Astronautics

(a)

(b)
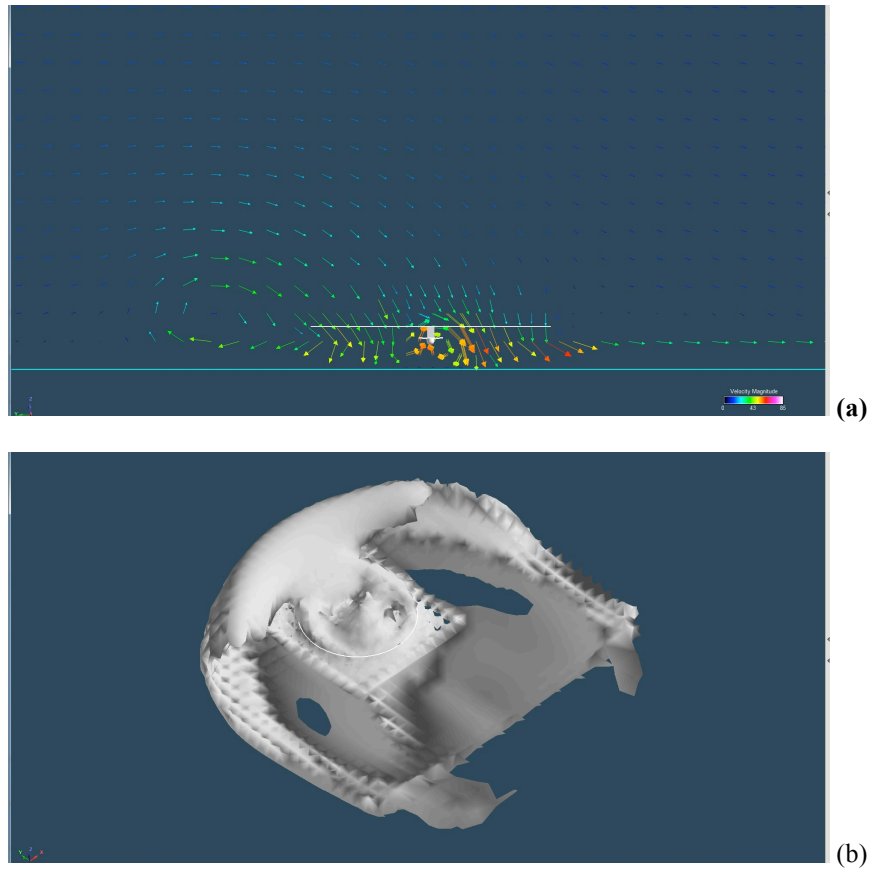
Figure 7. Single LCTR2 Rotor IGE with freestream velocity, V (h/R = 0.25): (a) flowfield vectors; (b) velocity magnitude isosurface (V=4m/s)

Figure 8 illustrates rotor performance characteristics of a single LCTR2 rotor IGE in edgewise-rotor forward-flight at a nominal thrust coefficient of C_T=0.012 (the same nominal conditions as to used to define the flow field images of Fig. 7). RotCFD does not currently have a rotor thrust trim option. Consequently, a matrix of rotor performance estimates needed to be made, at various different collective settings, so as to use linear interpolation to extract the power coefficient values for the target rotor thrust coefficient. Further, it should be kept in mind that no cyclic blade-root pitch-angle has been applied to the rotor to trim the rotor moments. The general rotor power coefficient trends are consistent with the original observations of Ref. 18 and the later Ref. 19 survey assessment as to the power trends for forward IGE. In this regards, there can be readily seen the influence of the ground-effect on the rotor power for low advance ratios (low forward-flight speeds); in turn as the advance ratio increases the influence of the ground effect quickly diminishes. RotCFD also successfully predicts the secondary rotor power trend effect wherein for certain h/R ratios the rotor power required could actually increase above that required for hover IGE for low advance ratios.
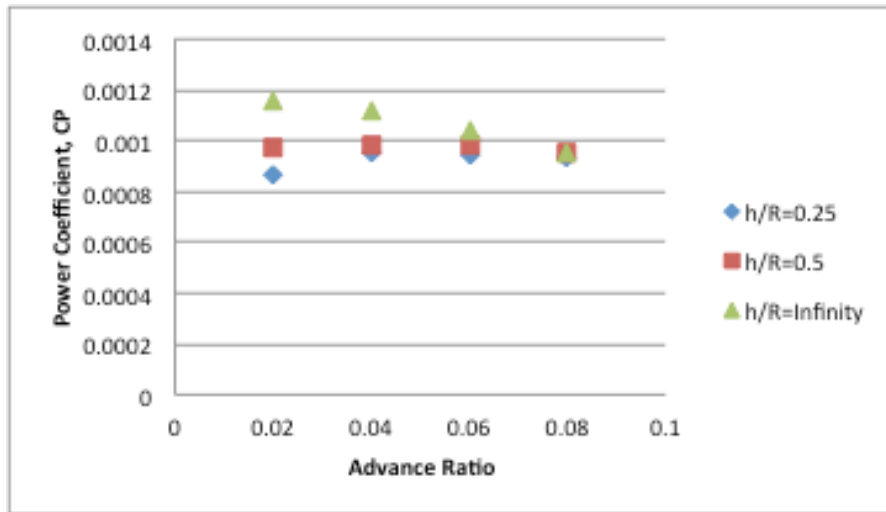
Figure 8. Single LCTR2 Rotor In-Ground-Effect with a Freestream Velocity (with a resulting effective advance ratio) at a fixed C_T=0.012.

A more direct comparison of the RotCFD forward-flight IGE predictions to the classic work of Ref. 18 can be accomplished by considering the rotor thrust trends for a single rotor. Figure 9 illustrates such a first-order comparison between classic rotor performance analytical theory and the RotCFD predictions.
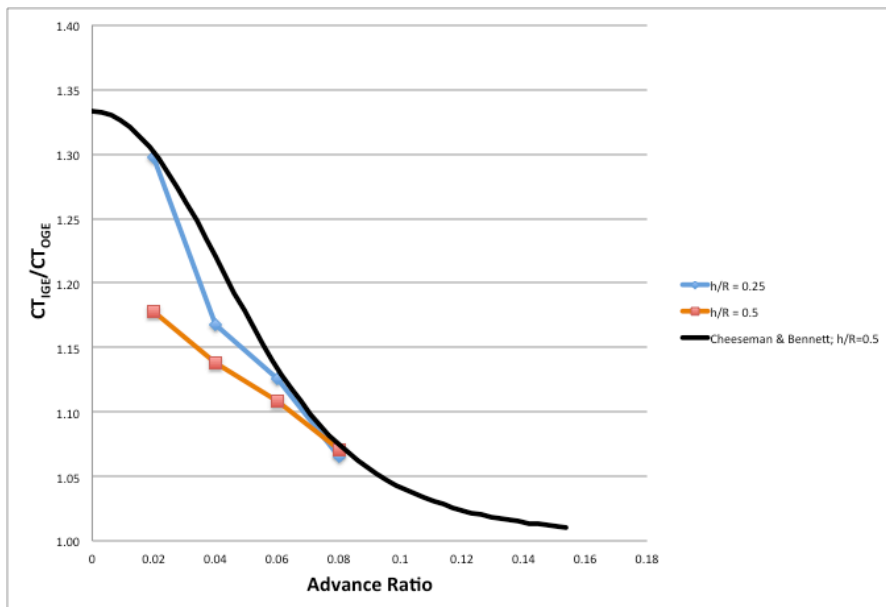
Figure 9. Single LCTR2 Rotor In-Ground-Effect with a Freestream Velocity

Figure 10 illustrates the hover IGE rotor performance trend of a single LCTR2 rotor (as earlier presented in Fig. 6, for a collective of twenty deg.) as compared to both dual rotors and the LCTR2 vehicle (rotor thrust only and not including airframe download). The figure-of-merit results are only shown for h/R≤1 for all three configurations, as all three configurations suffer from the (assumed) spurious fluctuations observed in the preliminary RotCFD results (for version 9.11) for h/R>1. Such spurious results are likely to stem from inadequate gridding refinement levels prescribed for the rotors and/or the earlier remarked-upon inadequacies for the stall-delay models currently used in the analysis. This is an area for future study.

Within the range of for h/R≤1, the RotCFD results in Fig. __ suggest that the IGE figure-of-merit trends for the single and dual rotor configurations are approximately the same. The IGE figure-of-merit values for the LCTR2 vehicle show a slight increase over the single/dual-rotor configurations; this is due to the anticipated "partial ground effect" of the vehicle fuselage and wing on the rotor performance. As the wing "body-fitting" refinement levels are admittedly set fairly low in the RotCFD model results presented herein, likely the wing "partial ground effect" contribution is understated in the presented results.
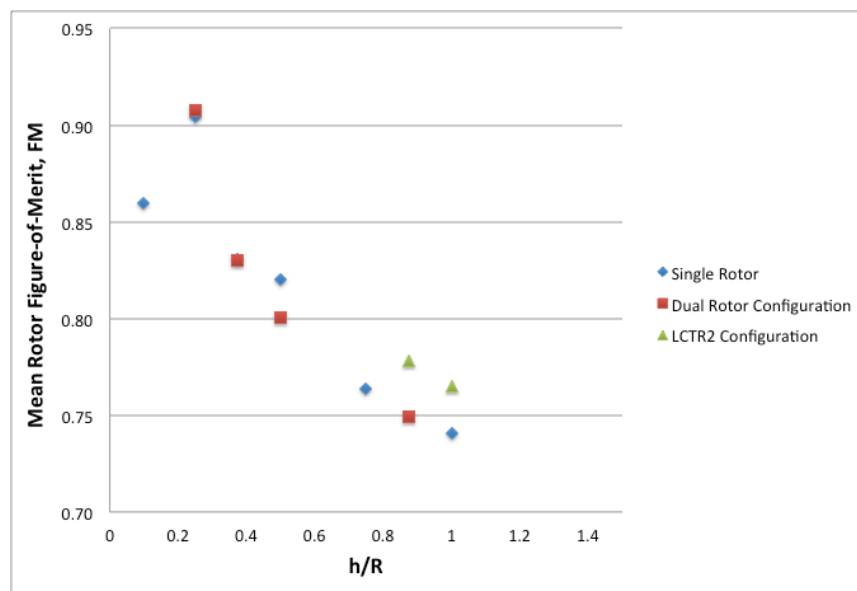
Figure 10.   Hover IGE Rotor Performance Trends for Single Rotor, Dual Rotors, and LCTR2 Vehicle

Figure 11 is a comparison of the flow fields of the dual rotor configuration versus the complete LCTR2 vehicle. The well-known fountain effect over the wing, between the two rotors, is not properly captured because the wing "body fitting' refinement levels were set fairly low as previously noted.
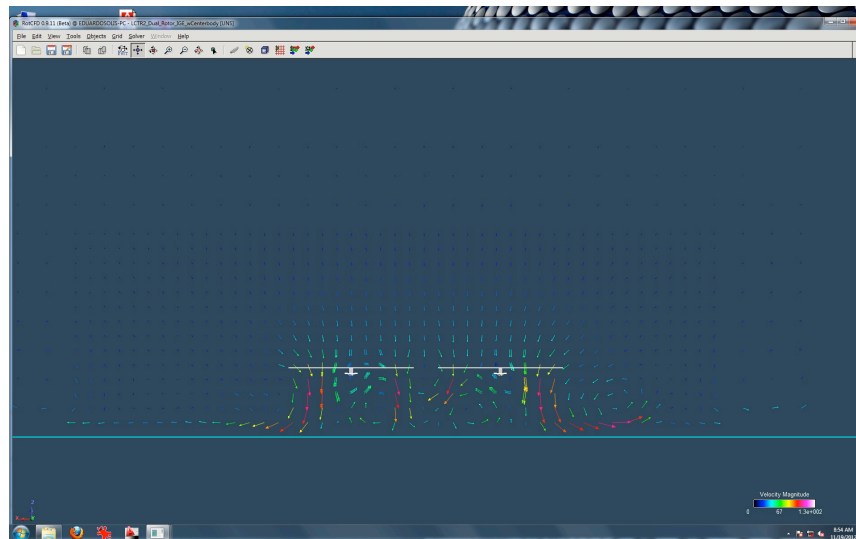
(a)
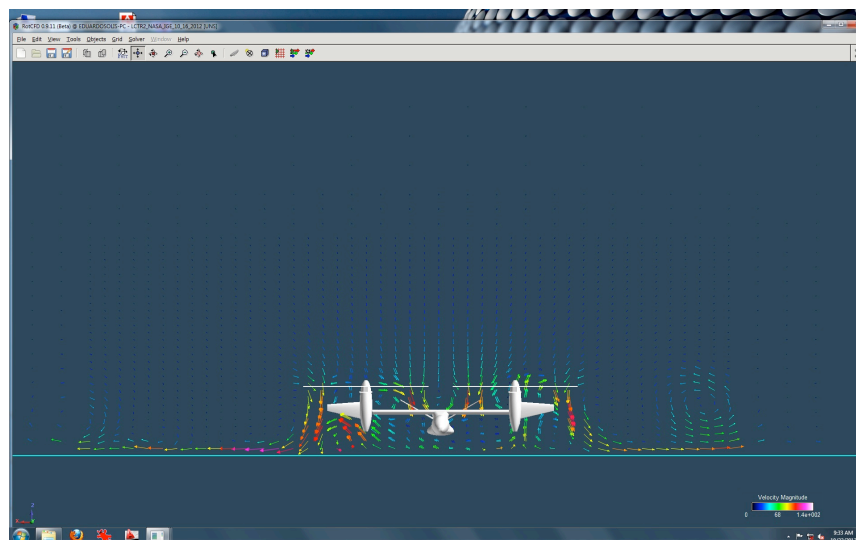
(b)

Figure 11.   Front View of Flow Fields of (a) Dual Rotor configuration and (b) LCTR2 Vehicle

B. Complete LCTR2 Vehicle Rotor/Wake Interactions with Ground and Side-Plane

As an initial, incremental step towards modeling the wake interactions of a civil rotor aircraft with vertiport terminal structures, a simpler, idealized modeling case is considered: the rotor wake interactions with both a ground and a side plane. The side plane represents, in an idealized sense, the close proximity of the civil tiltrotor with a very large (comparatively) building.

American Institute of Aeronautics and Astronautics
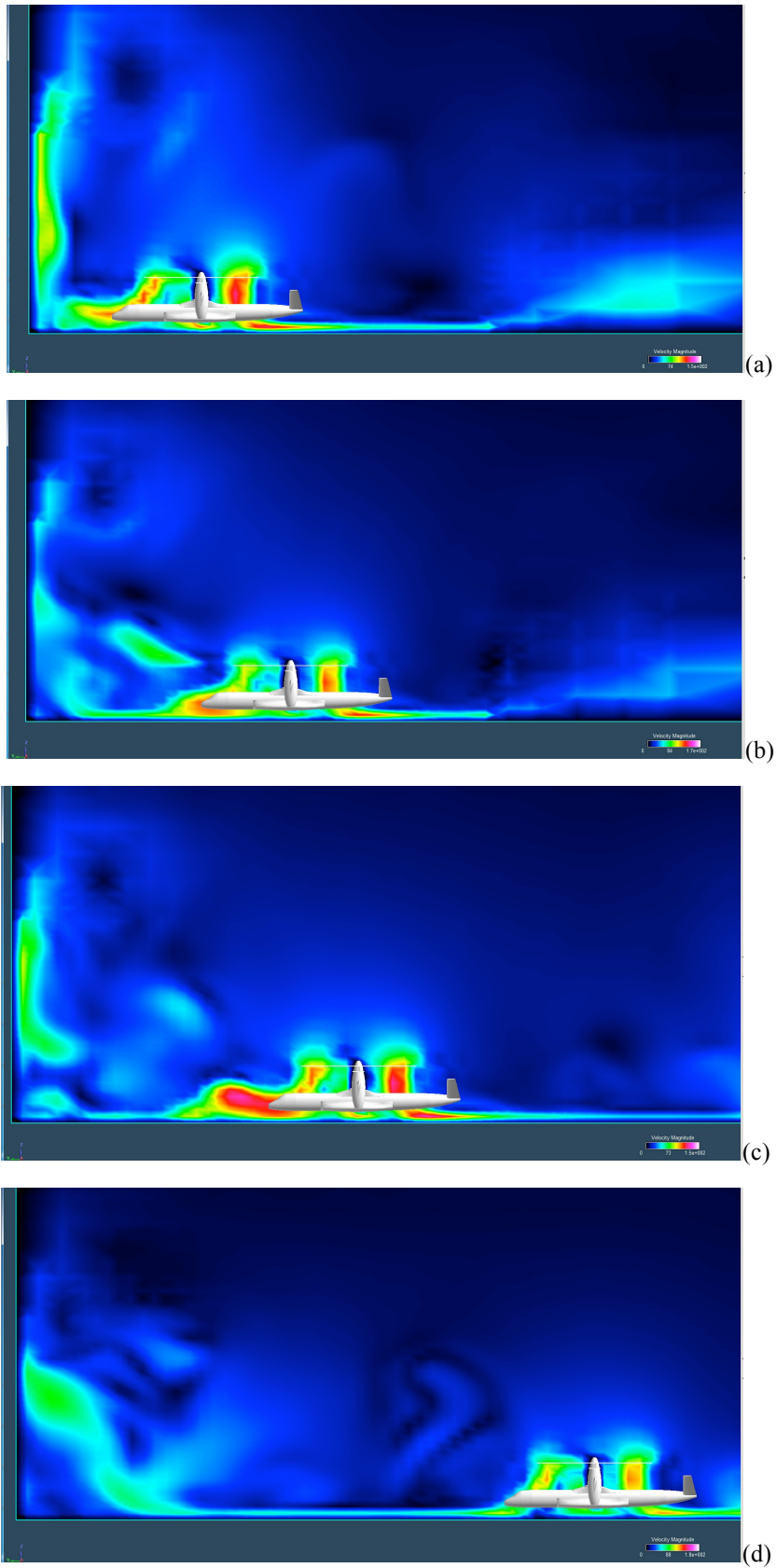
**Figure .   LCTR2 with Ground- and Side/Wall-Plane (h/R=0.875): (a) x/R=3;
(b) x/R=4.58; (c) x/R=6; (d) x/R=10**

American Institute of Aeronautics and Astronautics

RotCFD hover figure-of-merit results for a longitudinal distance (3≤x/R≤) sweep -- between the LCTR2 rotor vertical axes and the side-plane – at h/R=0.875 is shown in Fig. __. A small influence on x/R on the mean (the average of the two rotors) rotor figure-of-merit performance is observed.
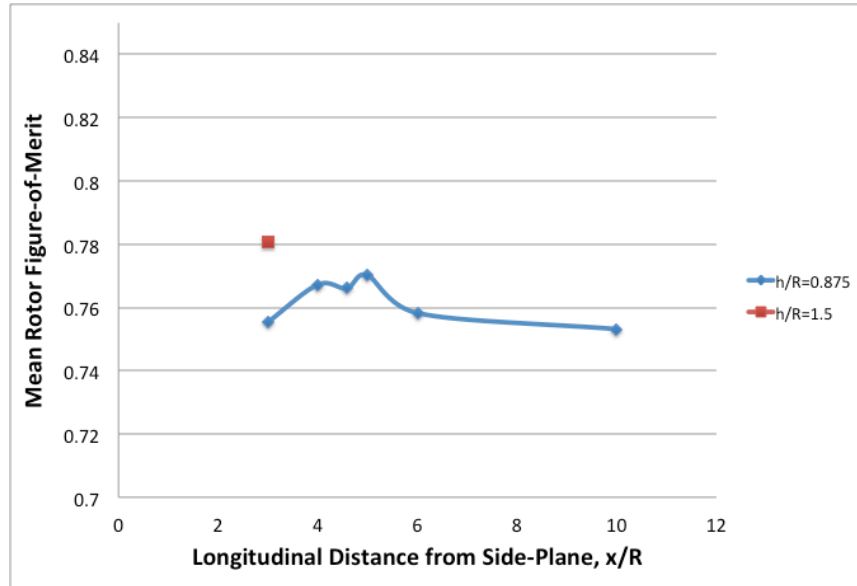
Figure .   Hover IGE rotor performance x/R trends for LCTR2 vehicle near a side-plane

Figure __ illustrates the wake interaction effects as the LCTR2 model is pivoted about the right hand rotor axis (yaw angle), such that the left hand rotor is moved further aft from the side-plane.   This pivoting, or yawing, of the LCTR2 aircraft model results in changes to the recirculation flow behavior next to and above the rotors.
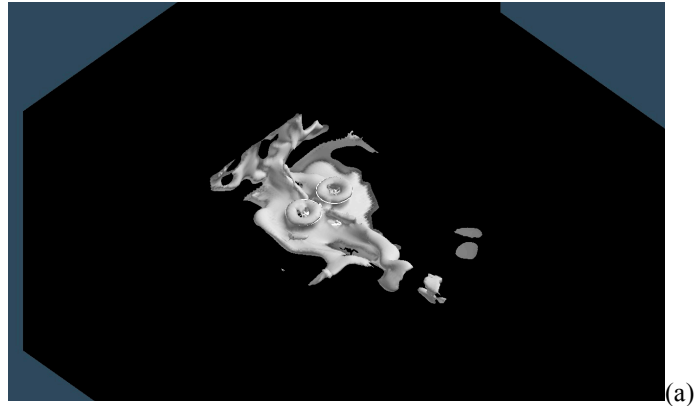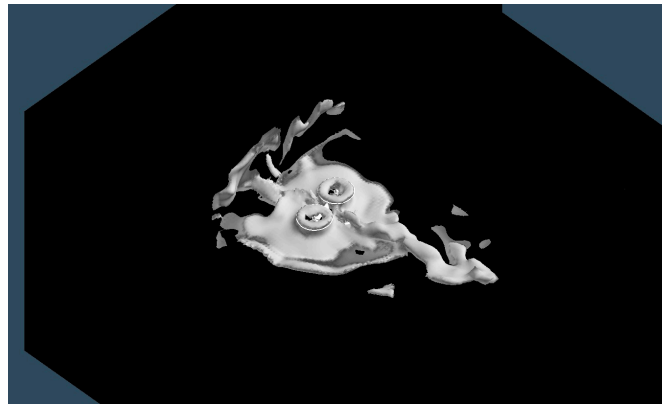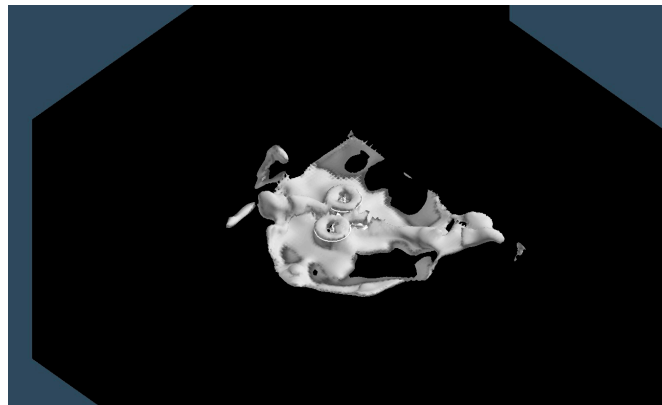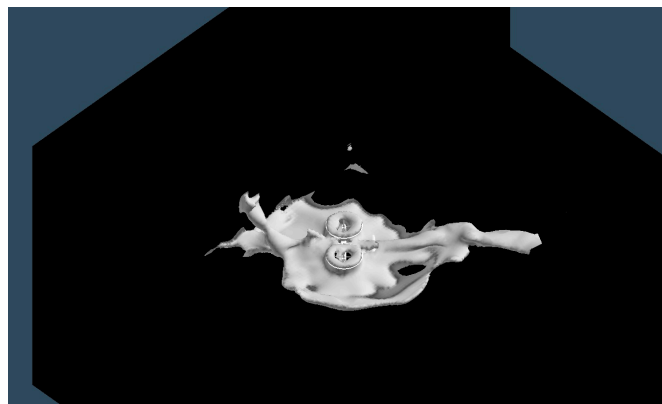
Figure . **LCTR2** **with** **Ground-** **and** **Side/Wall-Plane**
(h/R=0.875 and x/R=4): (a) Yaw Angle = 0 Deg.; (b) Yaw = 15
Deg.; (c) Yaw = 30 Deg.; (d) Yaw = 45 Deg.

Figure __ presents RotCFD results for the nondimensional rolling moment contribution from just the rotors (not the wings and fuselage) as the LCTR2 is yawed with respect to the side-plane.
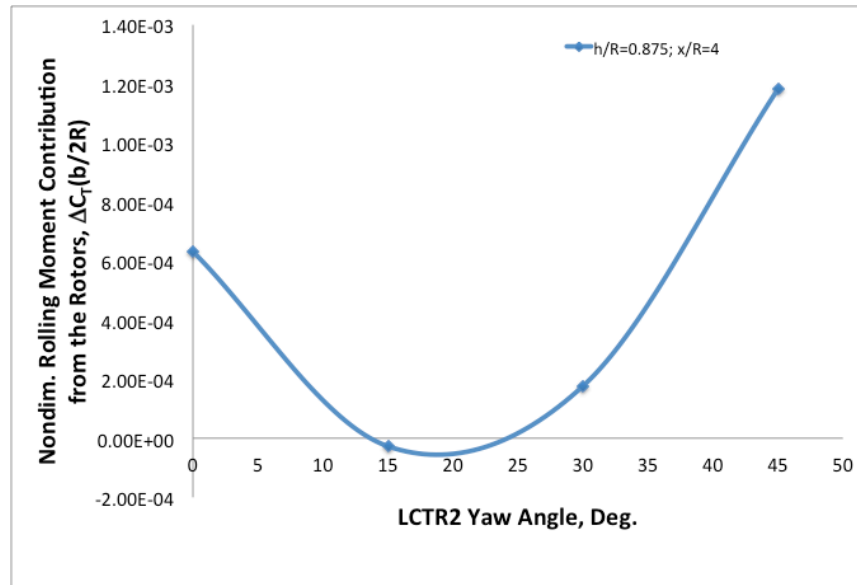
Figure .   Nondimensional rolling moments contributions from the rotors for the LCTR2 model in hover IGE in close proximity to a side-plane

C. Resulting Wake Interactions for Vertiport Configuration Permutations

Figure 4a-b illustrates one partial sweep of the LCTR2 aircraft, near a notional vertiport terminal, where the height above ground of the vehicle is varied. In Fig. 4, the LCTR2 vehicle is initially in ground effect and then rises out of ground effect as the vehicle height increase.   In the cases where the vehicle is in IGE the rotor groundwash significantly interacts with the vertiport terminal building. Key metrics in the final paper will be the location, direction, and magnitude of the maximum groundwash velocities predicted as well as, in the cases where vertiport buildings are modeled, the maximum and minimum surface pressures predicted on such notional buildings.

(a)

(b)

(c)
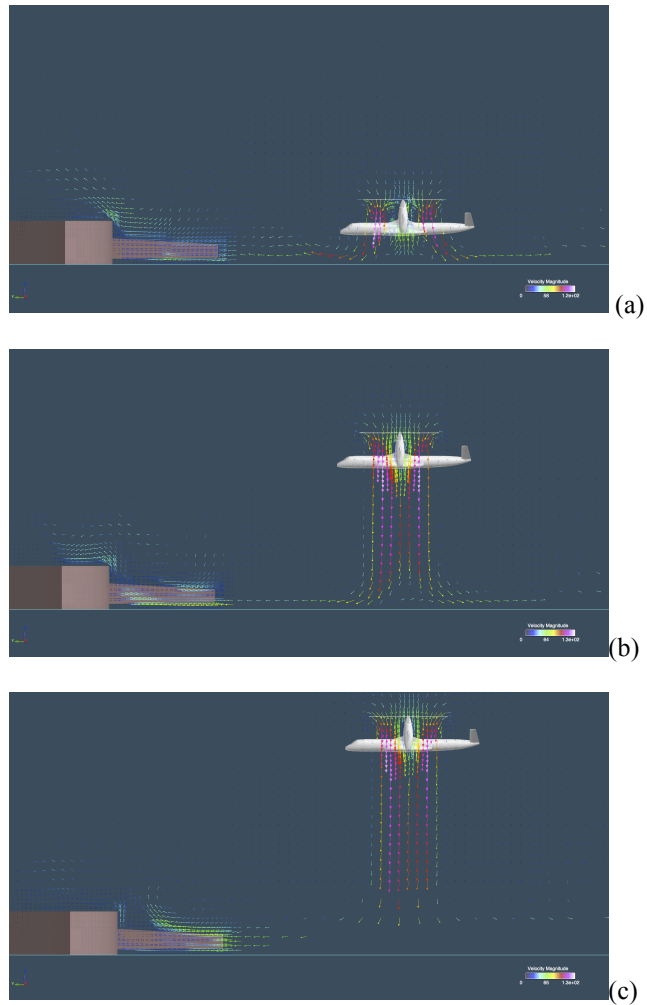
Figure 4. Height Sweep of LCTR2: (a) h/R=1.39; (b) h/R=4.16; (c) h/R=5.70.

Though not necessarily operationally recommended for civil tiltrotor vertiport CONOPS, Fig. __ presents some flowfield predictions of a LCTR2 over-flight over a vertiport terminal building during simulated takeoff .
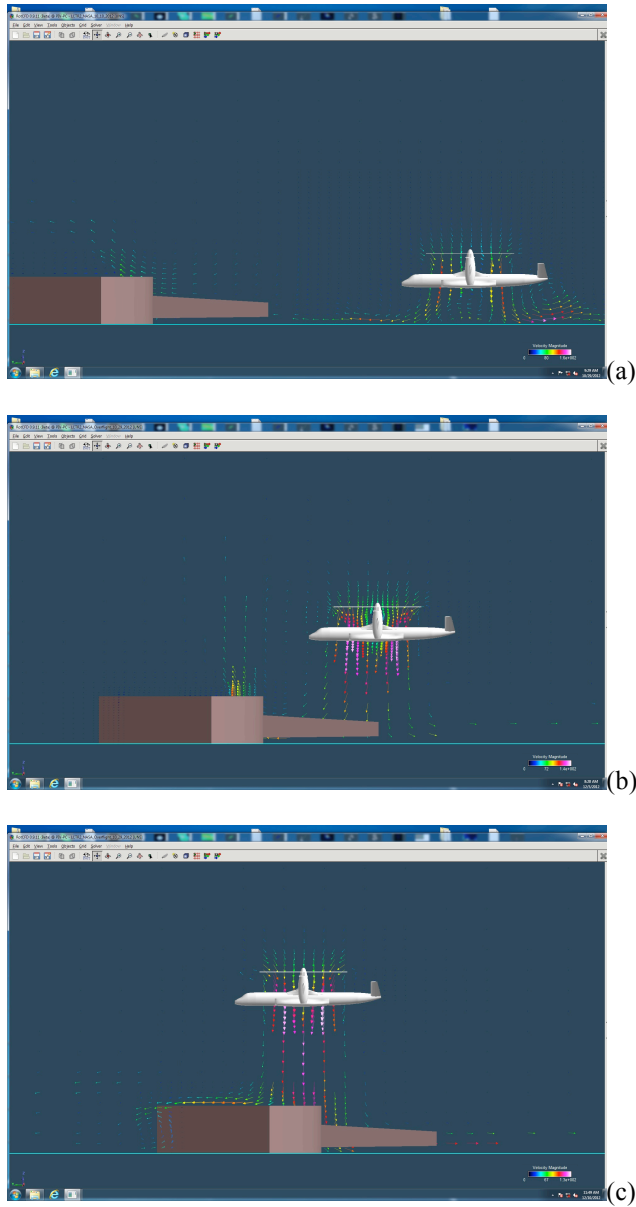
Figure . Over-flight of LCTR2 over a notional vertiport terminal building: (a) h/R=1.5 and x/R=4.58; (b) h/R=3 and x/R=0; (c) h/R=4 and x/R = -3.

The consequence of such overflights over and near vertiport terminals is substantial pressure loading of the building structure. Such loading is clearly captured in Fig. _.
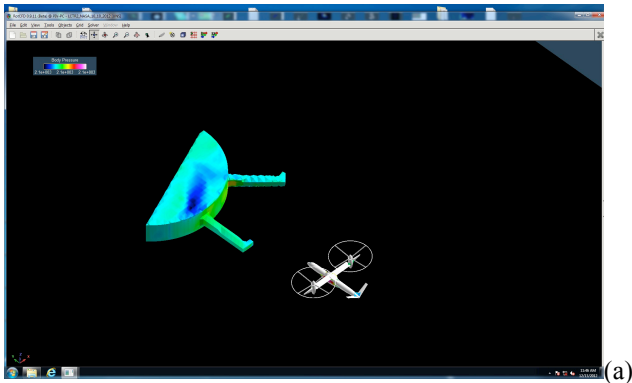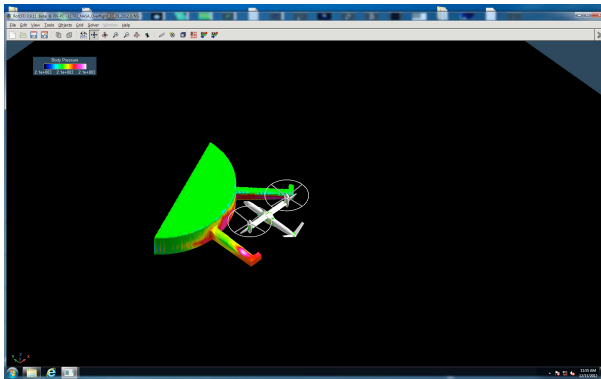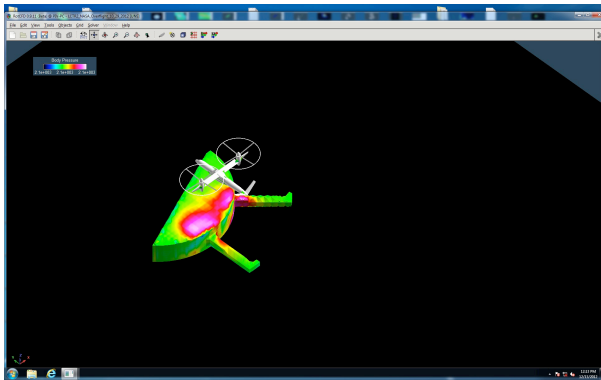
Figure .   Vertiport terminal building pressure loading due to over-flight of LCTR2: (a) h/R=1.5 and x/R=4.58; (b) h/R=3 and x/R=0; (c) h/R=4 and x/R = -3.

D. Additional Rotor/Wake Interaction Results for Surface-Equipment and General Aviation Aircraft

The ultimate outcome of this study is anticipated to be threefold. First, the information gleaned from this study will help refine future NASA reference designs for civil tiltrotor aircraft.   Second, the results from this study might help influence future vertiport design considerations.   Third, the results might also influence the concepts of operation of such vehicles in the airport environment such that the efficiency and safety of CTR operations at vertiports can be successfully balanced.

(a)

(b)

(c)

(d)
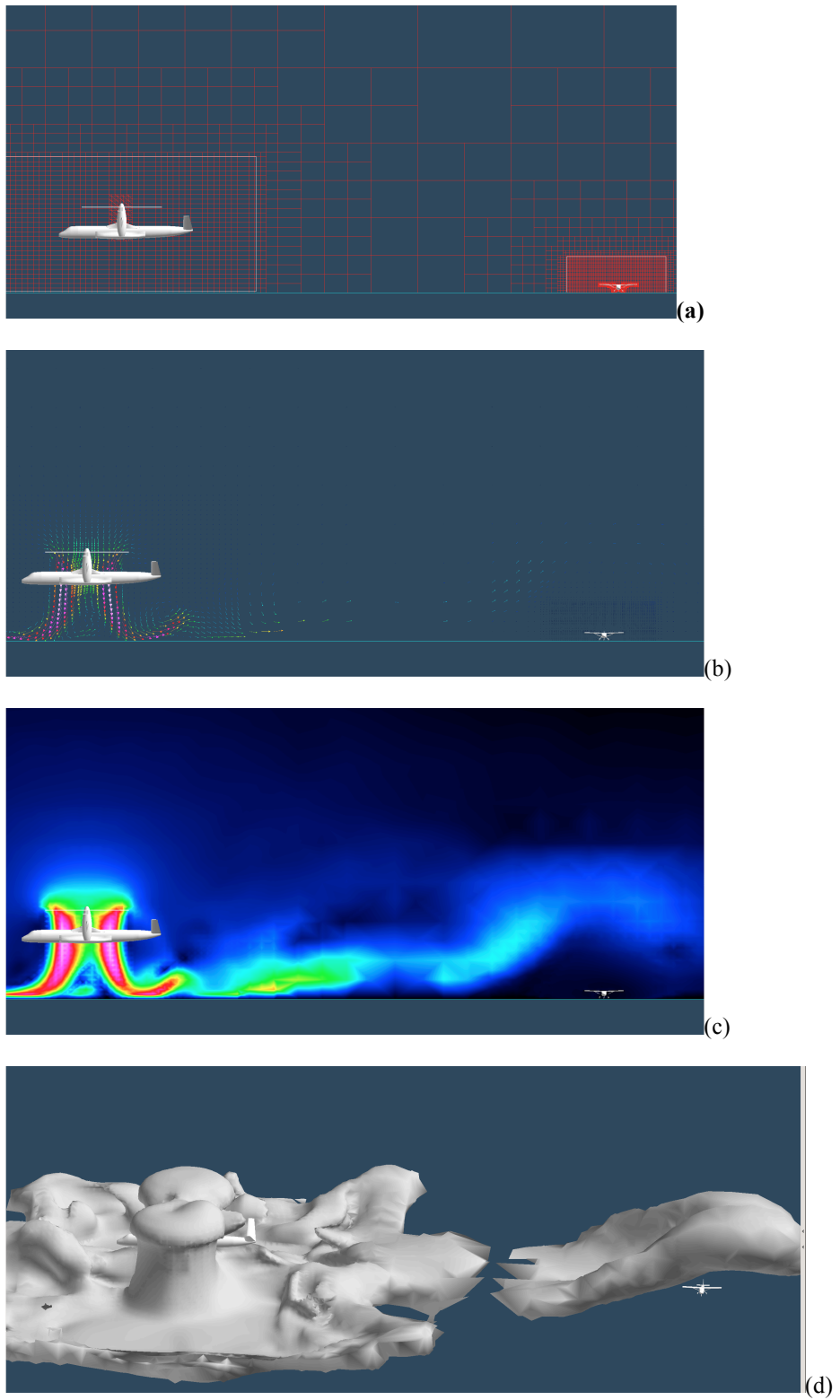
Figure .   LCTR2 Reference Design and Wake Interactions with Small General Aviation Aircraft

V. Concluding Remarks

A mid-fidelity computational fluid dynamics tool, one especially tailored for conceptual design studies of rotary-wing vehicles, is being applied to the problem of rotor/wake interactions (principally groundwash) in the vertiport environment. The rotor induced velocities from very large gross weight vehicles can be potentially hazardous and must be better understood. The results from this study are anticipated to help guide future NASA studies of the introduction of this new class of vehicles into the National Airspace System.

Acknowledgments

References

[1]Young, L.A., et al, "Civil Tiltrotor Aircraft Operations," 11th AIAA Aviation Technology, Integration, and Operations (ATIO) Conference, Virginia Beach, VA, Sept. 20-22, 2011.

[2]Young. L.A., et al, "A Study of Civil Tiltrotor Aircraft in NextGen Airspace," AIAA-2010-9106, 10th AIAA Aviation Technology. Integration, and Operations (ATIO) Conference, Fort Worth, TX, Sept. 13-15, 2010.

[3]Chung, W.W., et al, "Modeling High-Speed Civil Tiltrotor Transports in the Next Generation Airspace," NASA CR 2011-215960, October 2011.

[4]Patankar, S.V., *Numerical Heat Transfer and Fluid Flow*, Hemisphere Publishing Corp, New York, 1980.

[5]Rajagopalan, G., "RotCFD a Tool for Aerodynamic Interference of Rotors: Validation and Capabilities," Future Vertical Lift Aircraft Design Conference, San Francisco, CA, January 18-20, 2012.

[6]Acree, C.W., Yeo H. and Sinsay, J.D., "Performance Optimization of the NASA Large Civil Tiltrotor," Joint AHS/AIAA/SAE/RAeS International Powered Lift Conference (IPLC), London, UK, July 22-24, 2008.

[7]Young, L.A. and Derby, M.R., "Rotor/Wing Interactions in Hover," NASA TM 2002-211392, April 2002.

[8]Martin, P., "Tiltrotor/Building Interaction Test: 7x10 Wind Tunnel," Private Communication/Unpublished Data, May 2011.

[9]Rossow, V., "Effect of Ground and Ceiling Planes on Thrust of Rotors in Hover," NASA TM 86754, July 1985.

[10]Johnson, W., *Helicopter Theory*, Princeton University Press, 1980, pp. 122-124.

[11]FAA Advisory Circular, "Vertiport Design," AC # 150/5390-3, May 31, 1991.

[12]Light, J.S., "Tip Vortex Geometry of a Hovering Helicopter Rotor in Ground Effect," 45th Annual Forum of the American Helicopter Society, Boston, MA, May 22-224, 1989.

[13]Smith, R.D., Ed., "Heliport/Vertiport Design Deliberations: 1997-2000," DOT/FAA/ND-00/1, May 2001.

[14]Romander, E. A., Betzina, M., Silva, M., Wadcock, A. and Yamauchi, G. K., "Investigating Tiltrotor Formation Flight VIA 1/48-Scale Wind Tunnel Experiment," Proceedings of the American Helicopter Society 62nd Annual Forum, Phoenix, AZ, May 9-11, 2006.

[15]Yamauchi, G. K., Wadcock, A. J. and Derby, M. R., "Measured Aerodynamic Interaction of Two Tiltrotors," Proceedings of the 59th Annual Forum of the American Helicopter Society, Phoenix, Arizona, May 6-8, 2003.

[16]Johnson, W., Yamauchi, G.K., Derby, M.R., and Wadcock, A.J., "Wind Tunnel Measurements and Calculations of Aerodynamic Interactions between Tiltrotor Aircraft," 41st AIAA Aerospace Sciences Meeting, Reno, NV, January 6-9, 2003.

[17]Signor, D.B, Yamauchi, G.K., Smith, C.A., and Hagen, M.J., "Performance and Loads Data from an Outdoor Hover Test of a Lynx Tail Rotor," NASA TM 101057, June 1989.

[18]Cheeseman, I.C. and Bennett, W.W., "The Effect of the Ground on a Helicopter Rotor in Forward Flight," ARC RM 3021, 1955.

[19]Johnson, W., *Helicopter Theory*, Princeton University Press, Princeton, NJ, 1980; pp.146-148.

[20]Johnson, W., "Airloads and Wake Geometry Calculations for an Isolated Tiltrotor Model in a Wind Tunnel," Twenty-Seventh European Rotorcraft Forum, Moscow, Russia, September 11-14, 2001.

[21]Shih, T. H., Liou, W. W., Shabbir, A., Yang, Z. and Zhiu, J. (1995), " A New Eddy-Viscosity Model for High Reynolds Number Turbulent Flows-Model Development and Validation," Computers and Fluids, 24(3), pp. 227-238.

Appendix – Additional Validation Results

A. Reference 12 Single Rotor IGE Performance Results

One of the key experimental investigations into rotor wake interactions in-ground-effect was Ref. 12.
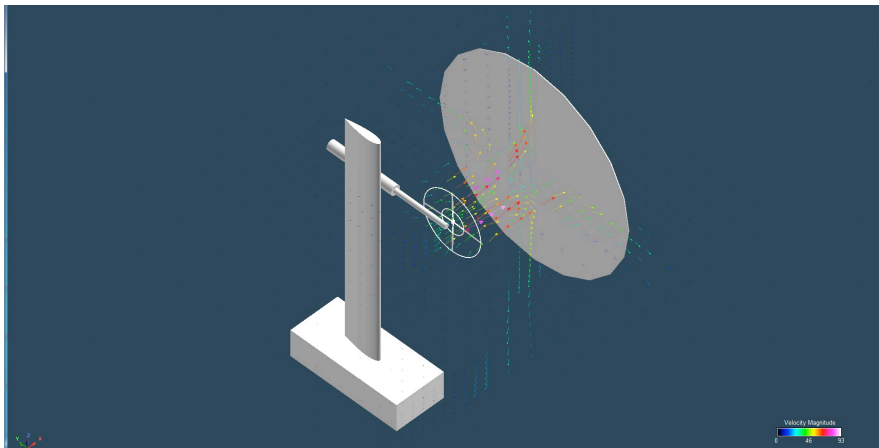
Figure . Representative RotCFD Flowfield Results for the Ref. 12 Test Configuration

The basic rotor hover performance predictive capability of RotCFD is highlighted next by performing RotCFD computations and correlating the results against Ref. 17 experimental data. The Lynx tail rotor tested in Ref. 17 was subsequently used in the in-ground-effect testing of Ref. 12 and, therefore, the Fig. __ OGE hover performance results have great pertinence to the subsequent IGE validation.   The Lynx tail rotor is particularly challenging to predict hover performance for, as it is a very high solidity rotor (σ=0.208) with a very large blade root cutout (r_c/R=0.384).   There has been, to date, very little work reported in the literature as to prediction/experimental correlation efforts for this rotor.   However, it is exactly this challenging nature of the problem that draws the authors of the current paper to this rotor and the Ref. 12 and Ref. 17 data sets.
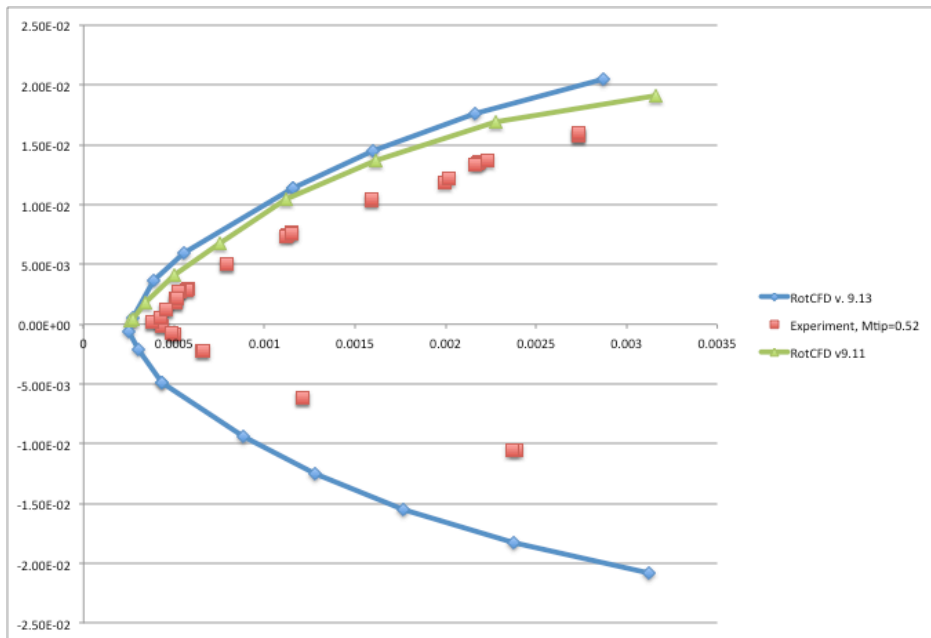
American Institute of Aeronautics and Astronautics

Figure .   Correlation between Experimental Results and RotCFD Predictions for the Lynx Tail Rotor CT vs. CQ trend

In discussing the validation of the hover in-ground-effect rotor performance predictions of RotCFD, it is necessary to consider subtleties between versions of RotCFD as well as modeling decisions related to rotor and body refinement levels as well as the expanse of the refinement boxes employed.   Figure __ summarizes a IGE rotor performance validation with respect to the Ref. 12 experimental data.
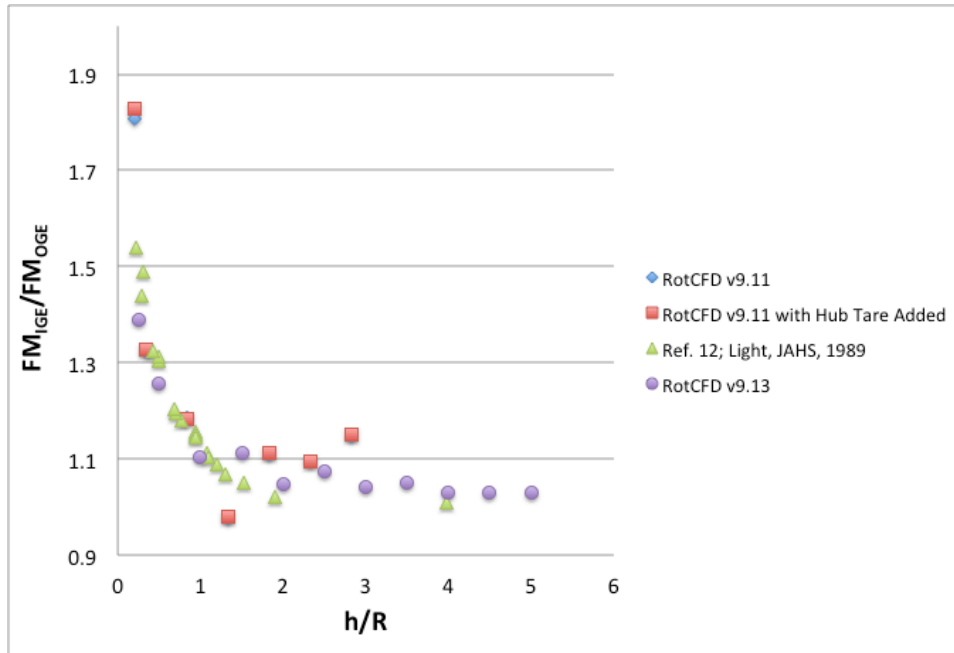
American Institute of Aeronautics and Astronautics

Figure .   Correlation between Experimental Results and RotCFD Predictions for the Lynx Tail Rotor In-Ground Effect for the Ratio of Figure of Merit IGE with respect to Figure of Merit OGE

B. Reference 13 Tiltrotor Aircraft Groundwash Velocities

An unique set of rotor outwash measurements was acquired in 1998 to support FAA research in vertiport/heliport operations. The outwash profile of a V-22 (e.g. Fig __) with wheels on ground and with the aircraft at several heights above ground are documented in Appendix A of Ref. 1. With wheels on the ground, profiles were measured in two directions: along the aircraft center line (azimuth = 0), and along an axis intersecting the two rotors on the port/left side of the aircraft (azimuth = 270 deg). Mean and peak velocities were measured in 1-ft increments above the ground between 1ft and 7 ft for four different aircraft thrusts.

Figure .   V22 Aircraft in Hover IGE

A RotCFD simulation was performed using two isolated V-22 rotors positioned at the same height as the V-22 wheels-on-ground experiment of Ref. 1. Figure xa) shows the two grid refinement boundaries within the computational domain. A cross-section of the grid system at x=0 is shown in Figure xb). As shown in Figs. xa) and xb), the domain boundaries were approximately Y = ±8D, X = ±6D, and Z = -0.56D to approximately 4D. The simulation was run for 21 simulated seconds. The solution at each of the last 5 seconds was saved and an average solution was computed from the five saved solutions. RotCFD does not currently have the capability to trim the rotors to a specified thrust, so a collective pitch was selected to provide a thrust level within the range (9950-33810 lb) measured by the experiment. For the simulation presented here, a collective pitch of 8.5 deg provided 23326 lb of thrust. Matching the measured thrust precisely was not critical as the correlation between experiment and simulation is presented using nondimenional parameters. The rotor diameter, D = 2R =38 ft, was used to nondimensionalize the distance from the aircraft centerline. The hover induced velocity, V_h = (aircraft thrust/$(4*\rho*\pi*R^2))^{1/2}$, was used to nondimensionalize the maximum mean velocity, Vmax$_{avg}$, from each velocity profile.


Figs. xa) and xb) present Vmax$_{avg}$/ V_h as function of the nondimensional distance in front of the aircraft and to the port/left side of the aircraft, respectively. As expected, the computed maximum mean velocity beneath or close to the rotors is not captured well since the fuselage, hubs, and nacelles were not modeled. However, at a distance of 2D from the the aircraft centerline, the computed Vmax$_{avg}$/ V_h tracks quite well with the measurements, except near Y=4D (Figxb)). Further grid refinements and incorporation of a representative fuselage, hub, and nacelle may improve the comparison closer to the rotor. Away from the rotor, however, the simple geometry of two isolated rotors provide a good approximation to the measurements.

American Institute of Aeronautics and Astronautics
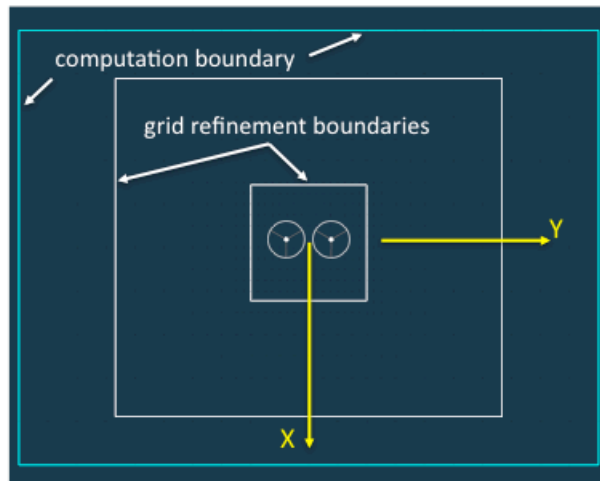
a) Top view of computational domain
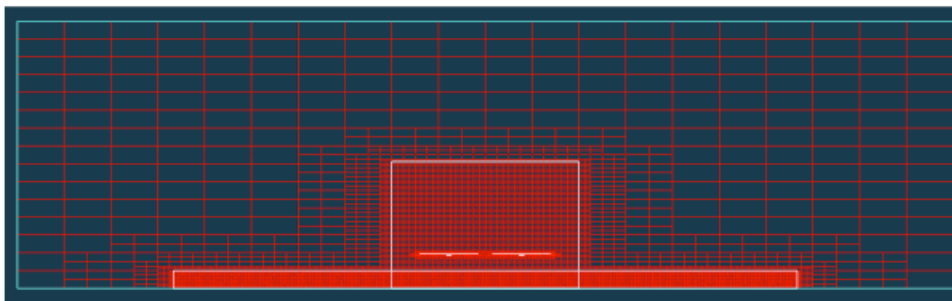
b) Front view of grid system at x=0
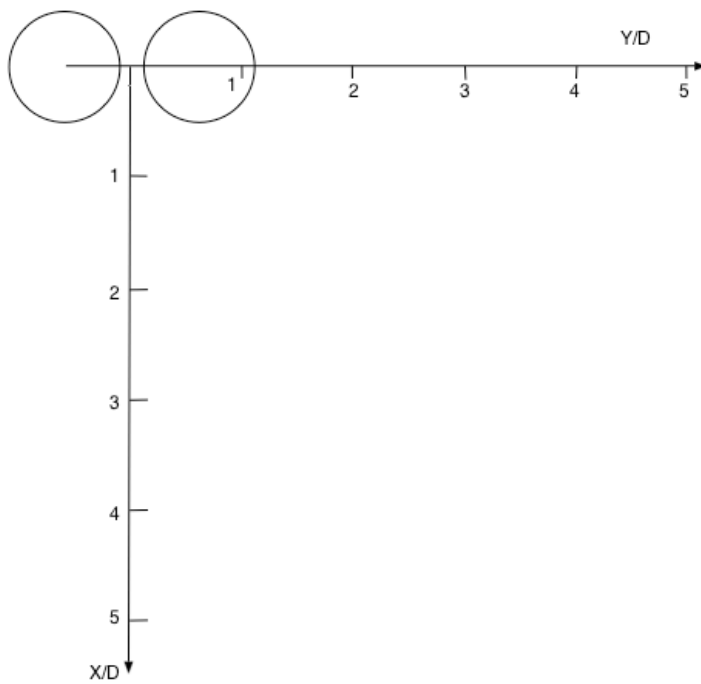
c) Non-dimensional coordinate system

Figure x. RotCFD computational domain and coordinate system.
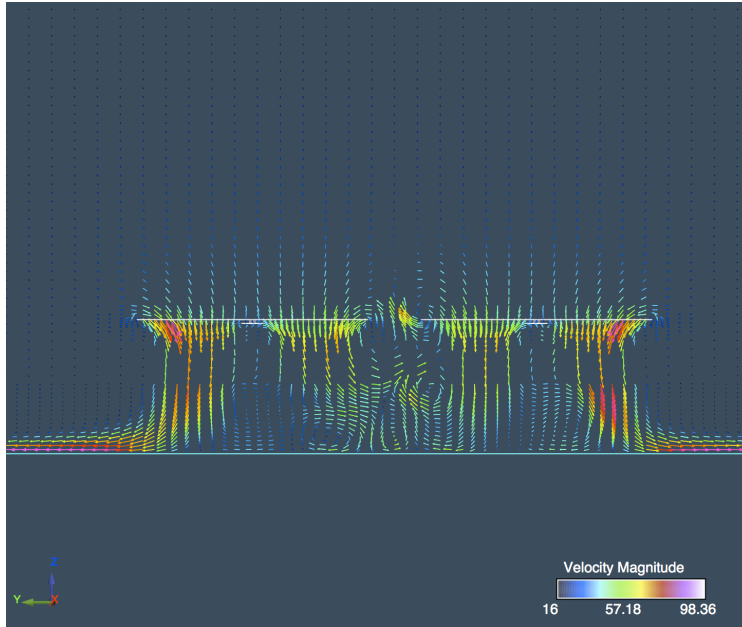
**Figure .   RotCFD predictions of a dual rotor configuration ()
flow field through the aircraft lateral plane, centered at the rotor
axes) consistent with the Ref. 13 Downwash/Groundwash Study**
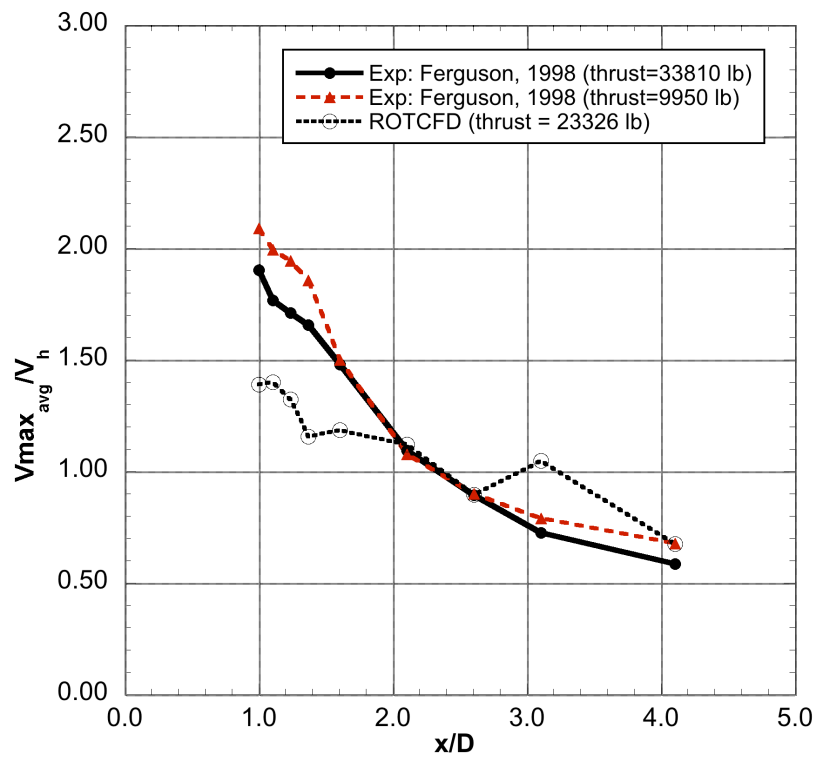
a) Maximum average velocity in front of aircraft along aircraft centerline (azimuth = 0 deg)
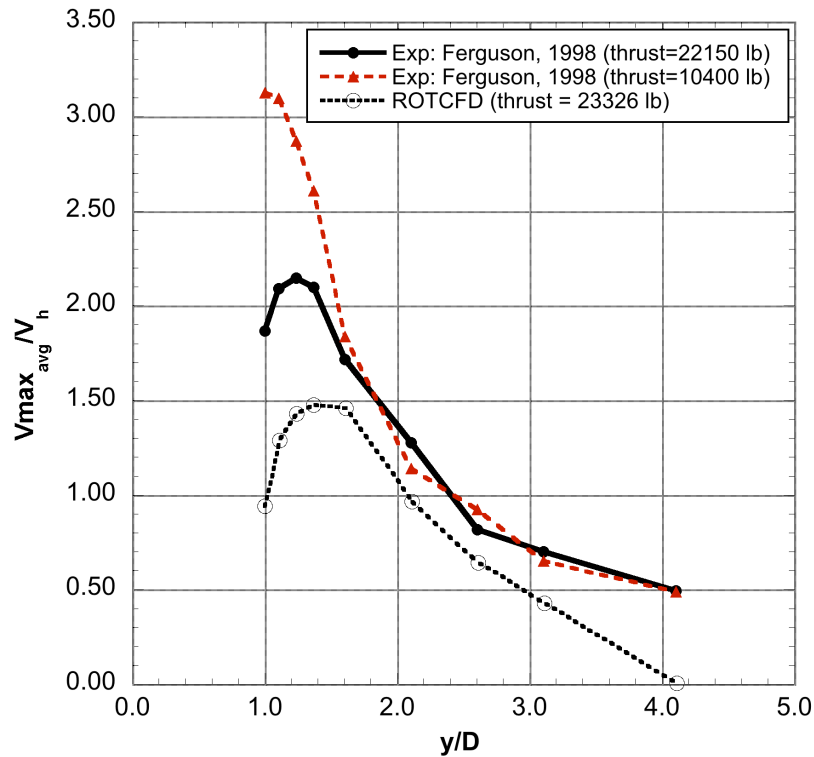
b) Maximum average velocity along axis passing through rotors (azimuth = 270 deg)

Figure x. Comparison of measured (Ref. x) and computed outwash velocities.

C. Reference 15 Small-Scale Tiltrotor IGE in Freestream Flowfield

During the early 2000's, a series of tiltrotor wake interaction studies were performed in the NASA Ames 7-by-10 Ft. low-speed wind tunnel. These wind tunnel tests employed several small-scale (~1/48th scale) tiltrotor test models. The majority of these small-scale tiltrotor tests focused on shipboard operations and aircraft formation flight but a few (e.g. Ref. 8 and 15) were directly relevant to the tiltrotor/vertiport wake interaction work of this paper. This appendix section will focus firstly on the performing RotCFD validation against experimental data from Ref. 15.

Reference 15 was primarily focused on tiltrotor aircraft formation flight aerodynamics' however, in the later sections of the paper a small portion of the discussion was focused on aircraft performance measurements in-ground-effect, during low-speed forward-flight (where the tiltrotor nacelles are in helicopter-mode and the rotors are in edgewise flight).

Figure .   Ref. 15 1/48th scale wind tunnel test model

As noted previously, the current versions of the RotCFD do not have an automated trim function. Therefore, accordingly, in order to match IGE/forward-flight data from Ref. 15 it was necessary to run a rotor collective sweep and then select a collective setting for the nominal CT set point used in the Ref. 15 data set (i.e. a trim condition of CT=0.012 at an advance ratio, μ, of 0.1).   Figure __ summarizes the rotor thrust and torque trends as a function of collective for the target advance ratio. Unfortunately, there is no comparable experimental data to validate these predicted performance trends.
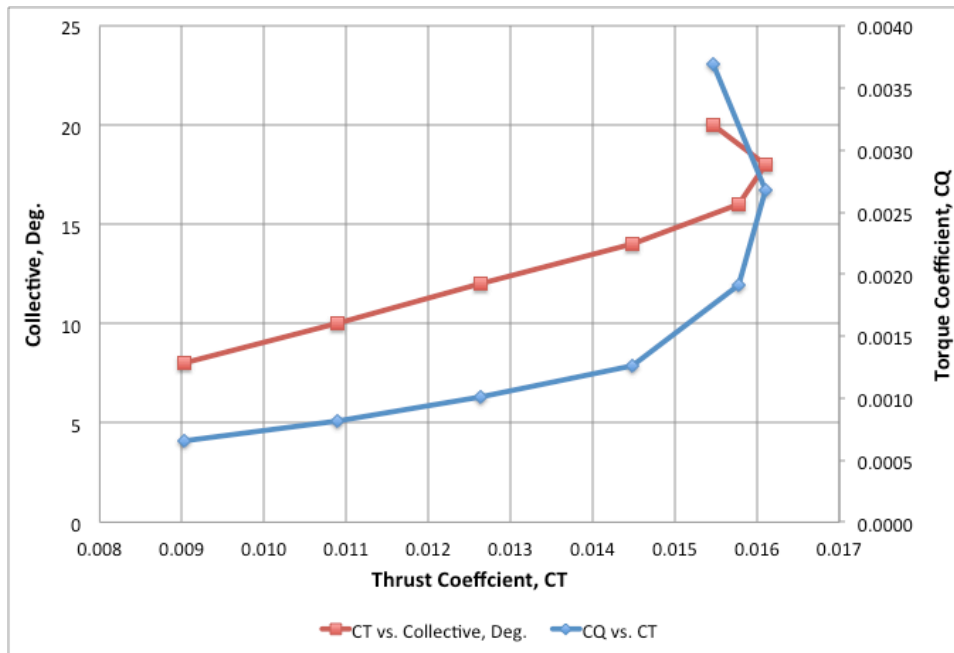
Figure .   RotCFD Predicted Thrust. Torque, and Collective Sweep at μ=0.1 for the Ref. 15 1/48th scale Tiltrotor Model

One of the key challenges of predicting the IGE in forward-flight conditions for the 1/48th scale tiltrotor, is as noted in Ref. 15, there was experimentally observed a laminar separation bubble originating near the lip of the wind tunnel ground plane used to simulate IGE during this test.   As a consequence of this separation bubble being manifested during the wind tunnel experiment, the rotor wake/boundary-layer/separation-buuble interactions appear to be pronounced for the wind-on experimental data.   RotCFD appears to be able to successfully predict the appearance of this separation bubble (e.g. the large blue areas displaced some distance above the ground plane in Figs. __ and __) but this somewhat subjective in that no wake flow visualization was reported in Ref. 15.   The CFD prediction problem is somewhat compounded by the fact that it is difficult to differentiate the boundary-layer recirculation observed in the RotCFD attributable to a separation-bubble versus that anticipated resulting from the horseshoe ground vortices being shed forward and below the rotors for small values of h/R.   RotCFD appears to predict separation bubbles just forward of, and underneath, the model's wing at both μ=0.05 and μ=0.1.

Another complication in correlating the Ref. 15 results with the RotCFD is that a fairly simple flat-plate wing representation that had to be used in these preliminary RotCFD predictions versus the 1/48th scaled V-22-like wing used in Ref. 15. Further, in Ref. 15 the rotor thrust coefficient values were derived from a model loading-measuring balance; this balance measured the total loads of the model and not just the rotor loads.   Tares then had to be taken in the Ref. 15 work so as to derive a measure of the mean rotor thrust.   It is unclear how, or if, the wing download was accounted for in the Ref. 15 rotor thrust coefficient values. This issue is of lesser importance for low, but nonzero, advance ratio test conditions. It is particularly crucial as to the hover IGE measurements presented.

American Institute of Aeronautics and Astronautics

(a)

(b)
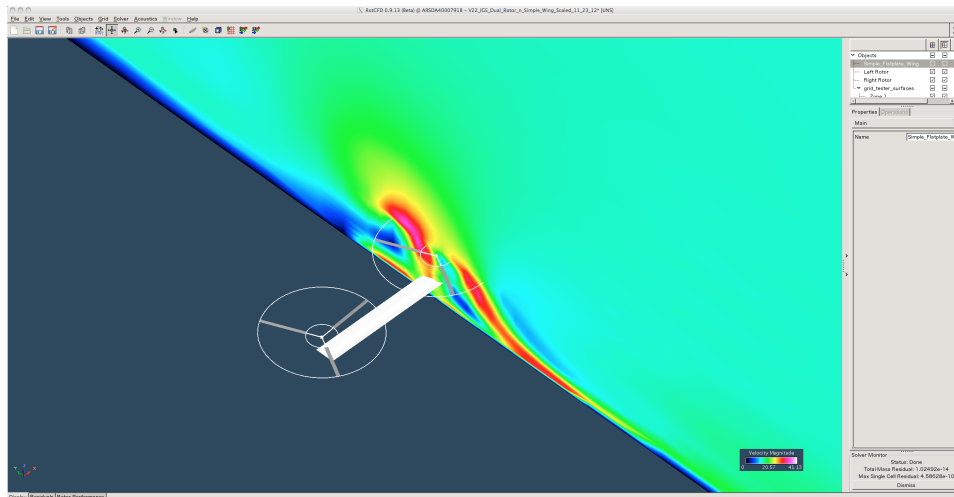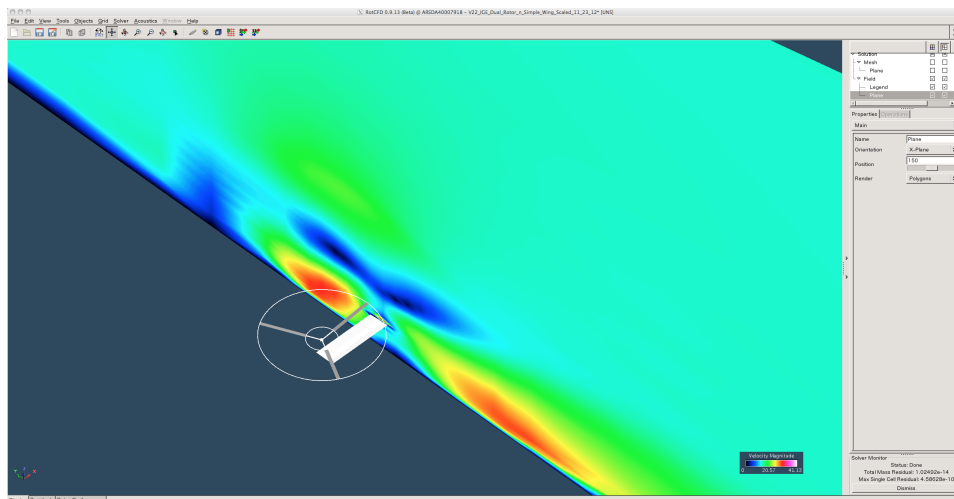
Figure .   RotCFD Small-scale Tiltrotor IGE/Freestream Interaction: (a) plane through right rotor and (b) through mid-span of wing (h/R=1 and μ=0.05)

American Institute of Aeronautics and Astronautics

(a)

(b)

Figure . RotCFD Small-scale Tiltrotor IGE/Freestream Interaction: (a) plane through mid-span of wing (h/R=1 and μ=0.1)
through right rotor and (b) through mid-span of wing (h/R=1 and μ=0.1)
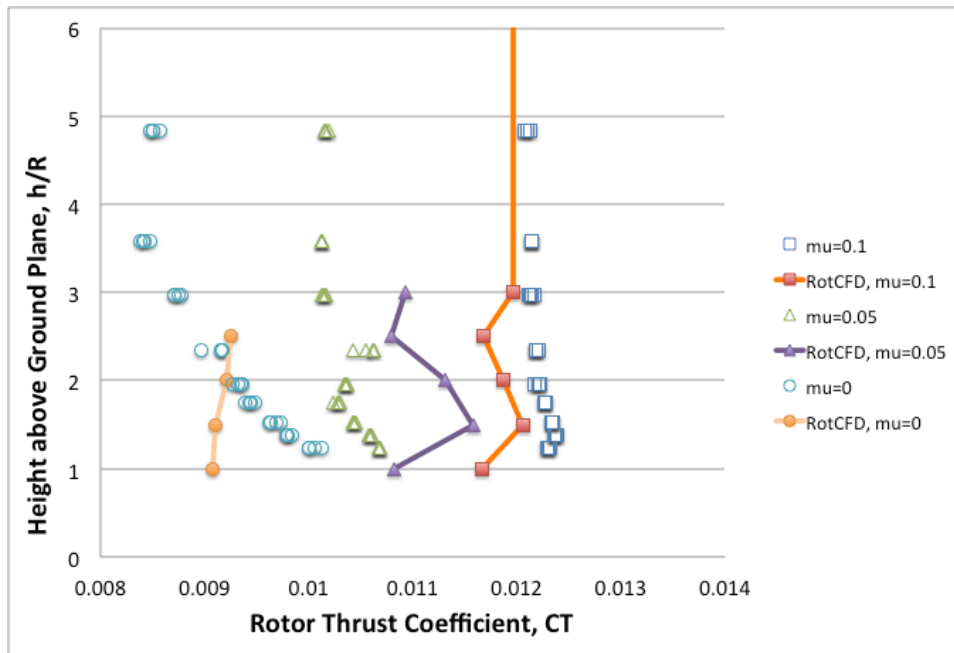
Figure . Correlation between Experimental Results and RotCFD Predictions for the Reference 15 1/48'th-scale Tiltrotor Model in IGE and Freestream Flowfield

The correlation results summarized in Fig. __ are mixed.

One final comment/observation related to the Ref. 15 RotCFD correlation is that with the simplified, flat-plate wing geometry it was possible to capture the well-known "fountain effect" for tiltrotor rotor/wing interactions.   The fountain effect recirculation flow patterns can be clearly seen above the wing, in the intermediate region between the rotor tips.
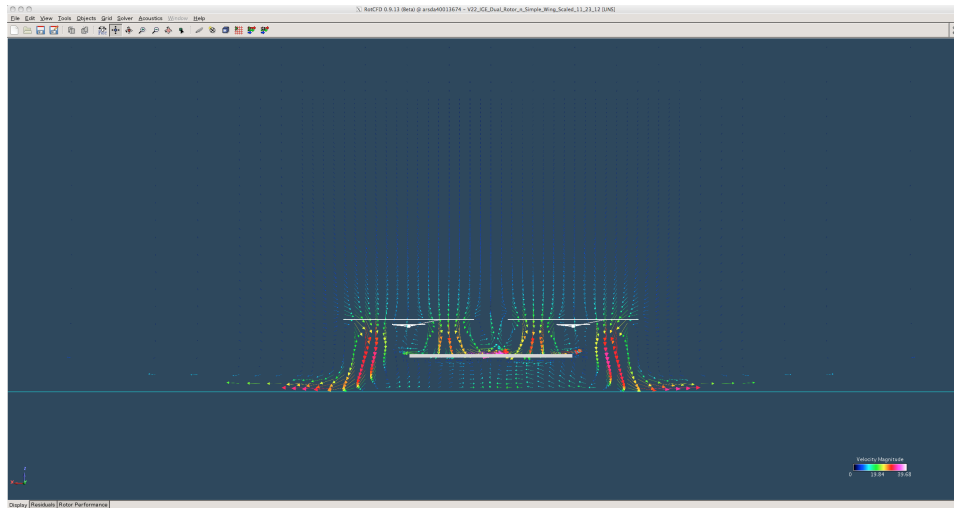
(a)
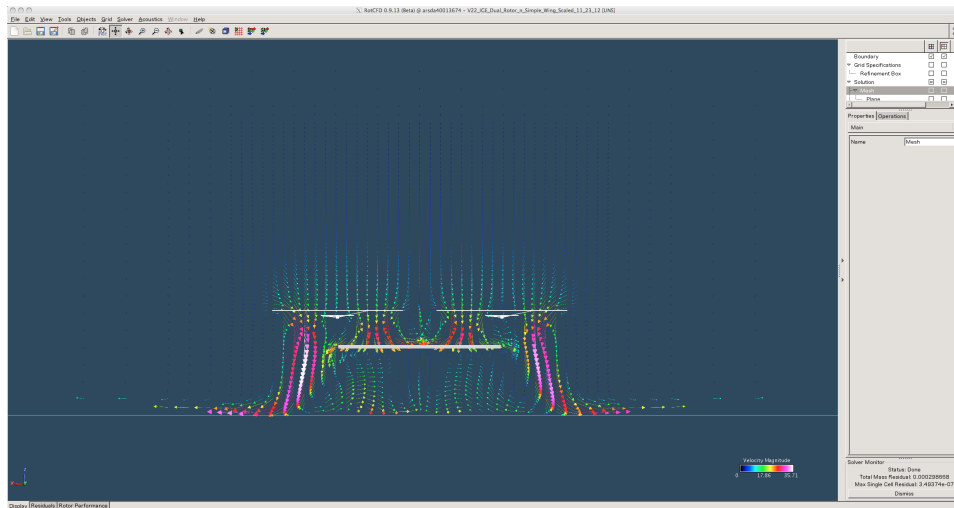
(b)
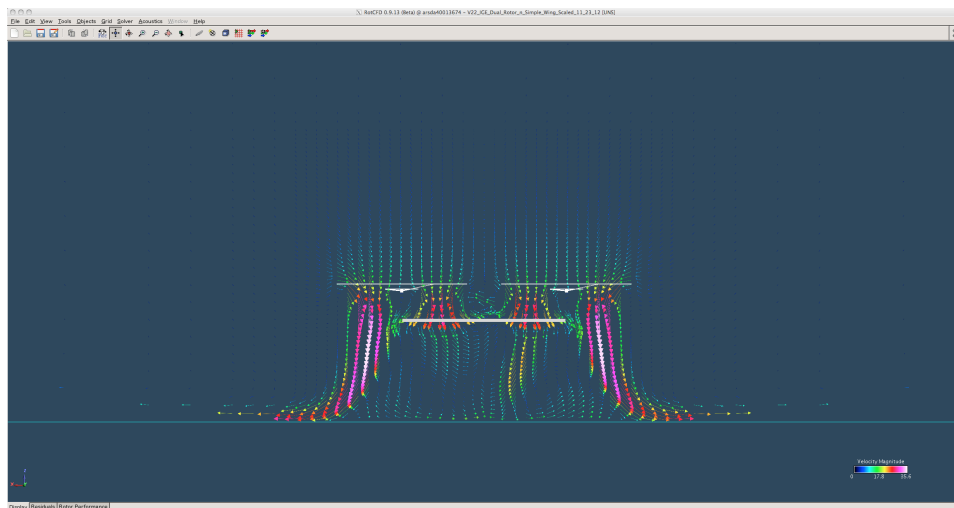
(c)

Figure .   RotCFD rotor wake wing and ground-plane interactions (with emphasis on the rotor/wing "fountain effect"): (a) h/R=1, (b) h/R=1.5, (c) h/R=2

D. Reference 8 Tiltrotor Aircraft and Building ("Urban Canyon") Interactions

Figure __ is a photograph of a wind tunnel experiment conducted in the 7-by-10 ft. test section, low-speed wind tunnel at NASA Ames Research Center. This test was conducted under the sponsorship of the then-existent NASA Vehicle Systems Program.


Figure . Small-scale Tiltrotor Aircraft Model (Mounted on a Sting) Downstream of a "Building" in the Wind Tunnel Test Section

Figure __ is the comparable RotCFD model of the tiltrotor and building wake interaction experiment shown in Fig. __.   Note that the wind tunnel sting is not modeled in RotCFD.   Tunnel-wall interference effects are also not modeled, though a ground-plane at the base of the simulated building is included.
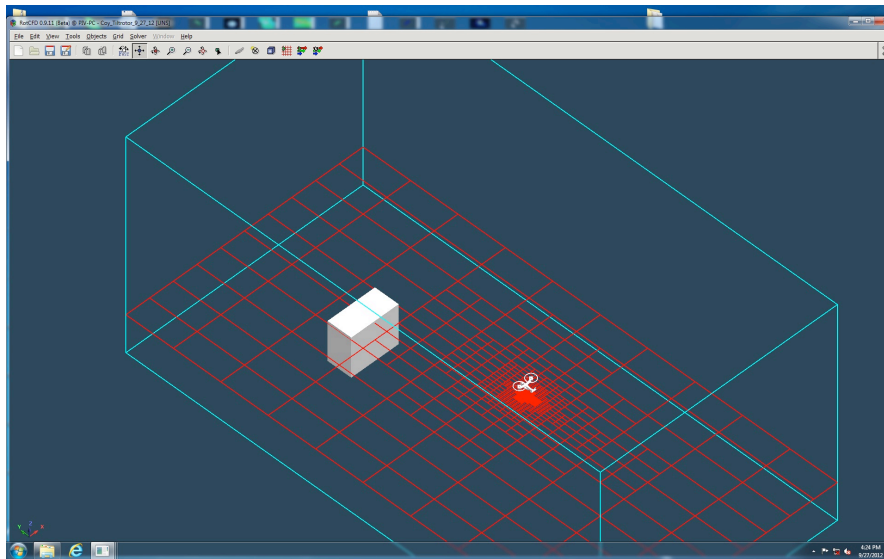
Figure . RotCFD Modeling of the Ref. 8 Building/Tiltrotor Wake Interaction Experiment
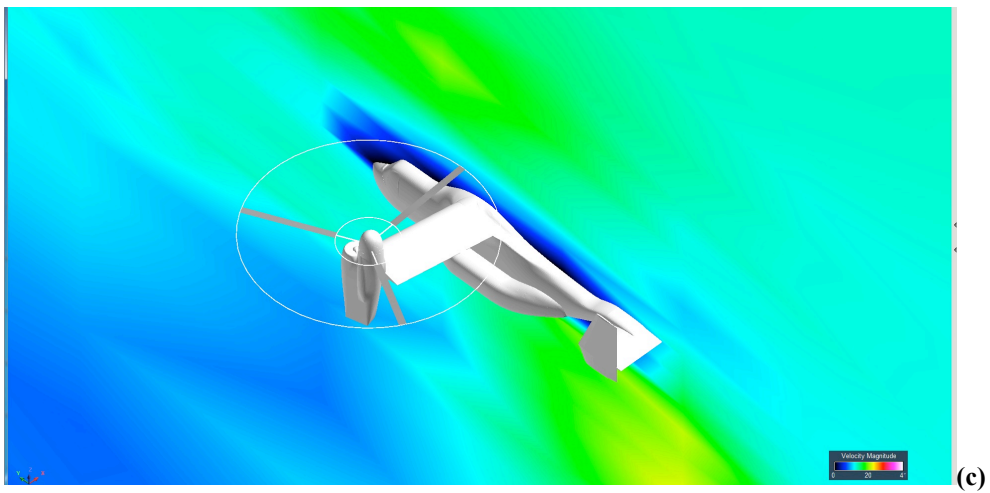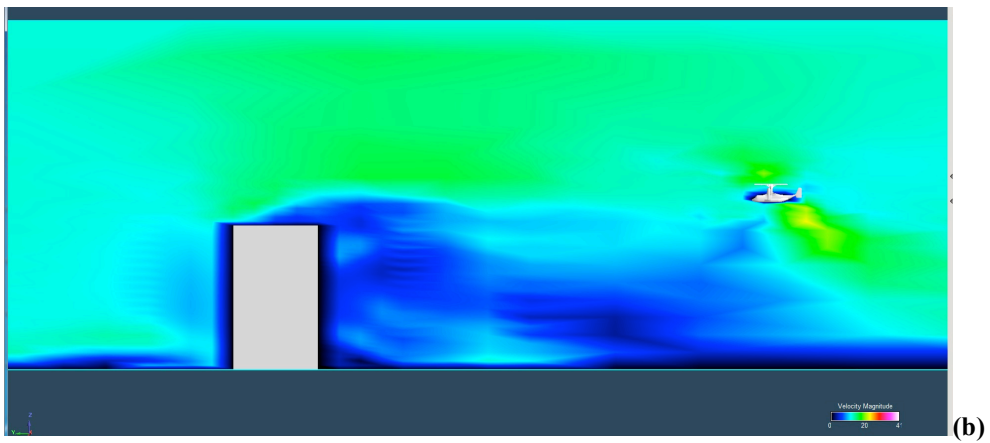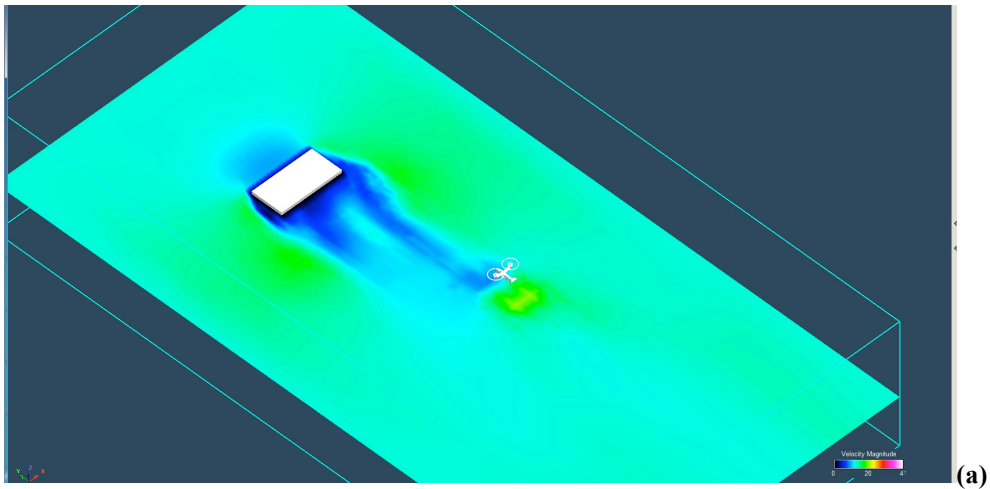
Figure .   RotCFD Prediction of Ref. 8 Building/Tiltrotor Wakes: (a) horizontal plane, (b) vertical plane and (c) close-up orthogonal view through mid-span of vehicle

Figures __ represent an initial correlation attempt to .

(a)   (b)
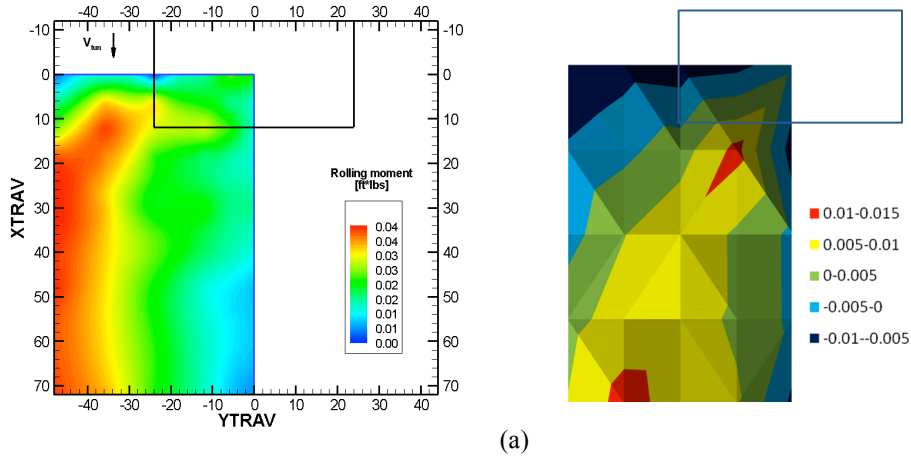
Figure 3. Ref. Tiltrotor/Building Wake Interaction: Influence on Vehicle Rolling Moment; (a) Experimental Data; (b) RotCFD Prediction.


(a)   (b)
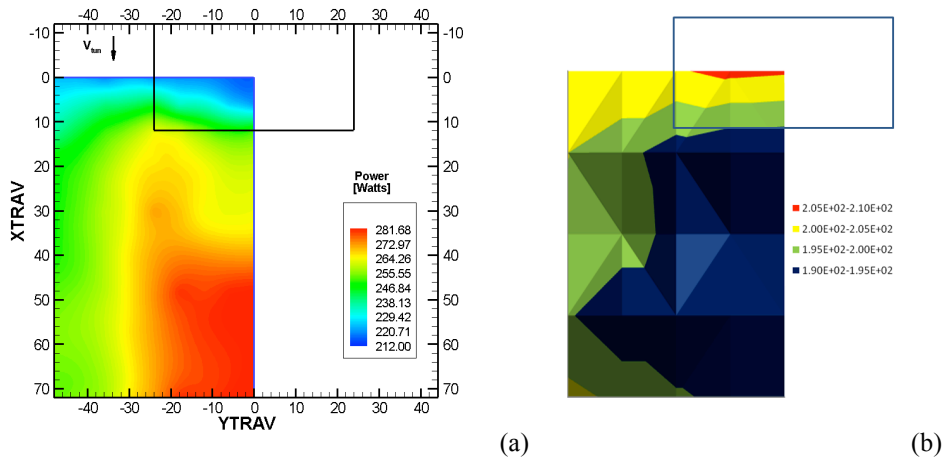
Figure 3. Ref. Tiltrotor/Building Wake Interaction: Influence on Vehicle Electrical Power; (a) Experimental Data; (b) RotCFD Prediction.

American Institute of Aeronautics and Astronautics

(a)   (b)
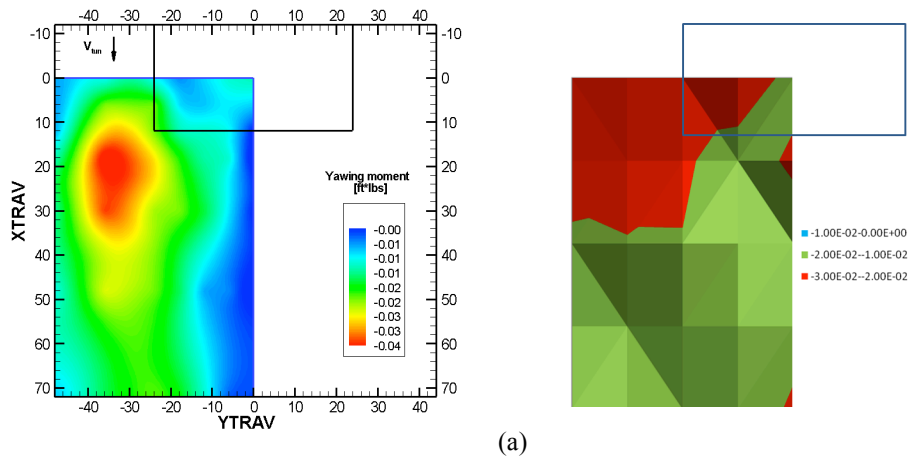
Figure 3. Ref. Tiltrotor/Building Wake Interaction: Influence on Vehicle Yawing Moment; (a) Experimental Data; (b) RotCFD Prediction.

American Institute of Aeronautics and Astronautics